



# Nanostructured Graphdiyne: Synthesis and Biomedical Applications

Ziqing Huang <sup>1,2,\*</sup>, Guanhui Chen <sup>3,\*</sup>, Feilong Deng <sup>1,2</sup>, Yiming Li<sup>1,2</sup>

<sup>1</sup>Hospital of Stomatology, Guanghua School of Stomatology, Sun Yat-sen University, Guangzhou, 510055, People's Republic of China; <sup>2</sup>Guangdong Provincial Key Laboratory of Stomatology, Guangzhou, People's Republic of China; <sup>3</sup>Department of Stomatology, Seventh Affiliated Hospital, Sun Yat-sen University, Shenzhen, 518107, People's Republic of China

\*These authors contributed equally to this work

Correspondence: Feilong Deng; Yiming Li, Department of Oral Implantology, Guanghua School of Stomatology, Hospital of Stomatology, Sun Yat-sen University, 56 Ling yuan xi Road, Yuexiu District, Guangzhou 510055, People's Republic of China, Tel +86 20 8386-3002, Fax +86 20-8382-2807, Email dengfl@mail.sysu.edu.cn; liym228@mail.sysu.edu.cn

**Abstract:** Graphdiyne (GDY) is a 2D carbon allotrope that features a one-atom-thick network of sp- and sp<sup>2</sup>-hybridized carbon atoms with high degrees of  $\pi$  conjugation. Due to its distinct electronic, chemical, mechanical, and magnetic properties, GDY has attracted great attention and shown great potential in various fields, such as catalysis, energy storage, and the environment. Preparation of GDY with various nanostructures, including 0D quantum dots, 1D nanotubes/nanowires/nanoribbons, 2D nanosheets/nanowalls/ordered stripe arrays, and 3D nanospheres, greatly improves its function and has propelled its applications forward. High biocompatibility and stability make GDY a promising candidate for biomedical applications. This review introduces the latest developments in fabrication of GDY-based nanomaterials with various morphologies and summarizes their prospective use in the biomedical domain, specifically focusing on their potential advantages and applications for biosensing, cancer diagnosis and therapy, radiation protection, and tissue engineering.

**Keywords:** graphdiyne, nanotechnology, biomedical applications

## Introduction

As one of the most abundant elements on Earth, carbon is widely applied in the fields of science and technology. There are three valence-bond hybridization states of carbon: sp, sp<sup>2</sup>, and sp<sup>3</sup>. Different forms of carbon atoms can combine together in many possible forms, producing various carbon allotropes with diverse morphologies and properties. For instance, diamond and graphite, two natural carbon allotropes consisting of an extended framework of sp<sup>3</sup>- and sp<sup>2</sup>-hybridized carbon atoms, respectively, possess highly different physical properties. To study specific properties and enrich the application of carbon allotropes, a large number of scientists have contributed efforts to the design and fabrication of novel carbon allotropes. Fullerenes, zero-dimension carbon nanostructures, were synthesized in 1985.<sup>1</sup> One-dimension carbon nanotubes were fabricated in 1991.<sup>2</sup> Graphene, a two-dimensional monolayer of carbon atoms, was constructed in 2004.<sup>3</sup> All of these synthetic carbon materials consist of sp<sup>2</sup>-hybridized carbon scaffolding and exhibit high conjugation and excellent electrical conductivity. Extensive theoretic and experimental research on novel carbon allotropes with different hybridized carbon atoms and their derivatives have prompted the development of the carbon family greatly.

Given this background, making full use of the three hybridized carbon atoms is of great significance. The structure and properties of graphdiyne (GDY) were firstly predicted by RH Baughman in 1987.<sup>4</sup> He estimated such planar carbon phases were comprised of sp- and sp<sup>2</sup>-hybridized carbon atoms with high expected stability. Consequently, scientists exerted great efforts to construct GDY via synthesizing monomeric and oligomeric substructures.<sup>5,6</sup> In 2010, Li et al successfully synthesized layer-like GDY film of 3.61 cm<sup>2</sup> via acetylenic cross-coupling reactions, which made the theoretically predicted GDYs reality.<sup>7</sup> GDY, comprised of coexistence of sp<sup>2</sup> and sp carbon, exhibits excellent conductivity, low carrier mobility and enhanced redox activity.<sup>8</sup> The natural bandgap of GDY facilitates it constructing novel nanosystems with adjustable electronic and optical properties. The triple-carbon bonds of GDY as potential active sites enable it to be functionalized via the covalent or noncovalent interaction

between GDY and other unsaturated ligands. Compared with other  $sp^2$ -hybridized carbon-based materials, GDY could remain its highly conjugated structure after functionalization, which contributes to modulating their properties for various applications.<sup>9</sup> Since its first synthesis, GDY has attracted increasing attention and recent research has found GDY and its derivatives ideal candidates for application in various fields, such as photocatalysis,<sup>10–12</sup> electrocatalysis,<sup>13,14</sup> energy storage,<sup>15–18</sup> and environment.<sup>19,20</sup> In addition, the hydrophobic interaction and  $\pi$ - $\pi$  stacking endows GDY with strong adsorption capacity, and thus GDY is able to load drugs, genes, tracking probes and biological macromolecules for versatile uses. Also, due to efficient drug-loading ability and photothermal conversion capacity, GDY has broad application prospects in cancer treatment and diagnosis. The extraordinary physical and chemical properties combined with better biocompatibility and biosafety than other 2D materials make GDY a promising candidate for biomedical applications.<sup>21</sup> To improve performance of GDY, synthetic techniques have been exploited to construct GDY with different well-defined nanostructures and distinctive properties. To date, GDY has been successfully prepared in various forms, such as nanotubes, nanowires and nanoribbons, and exhibits great prospects in the biomedical field, yet there is no detailed summary of development in synthesis of GDY-based nanostructures and their biomedical applications. Herein, we summarize new synthetic approaches for GDY with different morphologies, incorporating quantum dots, nanotubes, nanowires, nanoribbons, nanowalls, nanosheets, ordered stripe arrays and nanospheres. On this basis, recent progress of GDY-based nanomaterials in biomedical applications and advantages will be discussed.

## Synthesis

Design and synthesis of carbon-based materials with controllable size, shape and microstructures are significant to their properties and potential biomedical applications. Taking nanotubes, for example, their tunable lengths enable them to function as drug carriers and the ability to bind with antibodies with radio- or fluorescent labels makes them prominent in diagnosis. Photophysical properties of quantum dots, such as brightness and stability, offer potential for their applications as fluorescence imaging agents.<sup>22</sup>

The size and morphology of GDY is controllable by tuning experimental conditions like catalyst systems, selected templates and precursor characteristics in the process of preparation, which can greatly influence on its physical, chemical, and electronic properties and expand innovative application fields. Since its first bulk synthesis, multiple explorations have been made into synthesizing and tailoring GDY with different experimental conditions (eg, catalyst and selected template). GDY has been synthesized with novel nanostructures categorized as 0D quantum dots, 1D nanotubes/nanowires/nanoribbons, 2D nanosheets/nanowalls/ordered stripe arrays and 3D nanospheres (Table 1). In this section, recent achievement in fabrication of GDY with well-defined nanostructures and their distinct properties will be summarized.

**Table 1** Summary of synthetic methods for GDY

Morphologies	Method	Ref.
Quantum dots	Sonogashira cross-coupling reaction	[23]
Nanotubes	Anodic aluminum oxide template	[24]
Nanowires	Vapour–liquid–solid growth	[28]
	Vicinal surface template	[29,30]
Nanoribbons	Stepwise inter- and intramolecular Glaser–Hay coupling	[31]
Nanowalls	Modified Glaser–Hay coupling	[34]
	Copper envelope catalysis	[35]
Nanosheets	Liquid–liquid interface or gas–liquid interface	[37]
	In situ on copper nanowires	[17]
	Bipolar electrochemistry method	[39]
Ordered stripe arrays	Superlyophilic grooved templates	[40]
Nanospheres	Explosion method	[41]

## Quantum Dots

In 2020, Guo et al succeeded in preparing graphdiyne quantum dots (GDY-Py QDs) with strong fluorescence.<sup>23</sup> It was obtained by Sonogashira cross-coupling reaction in which pyrene groups were conjugated connected with GDY. The synthesized GDY-Py QDs possessed outstanding dispersibility in many solvents, including organic solvents and water, a high relative quantum yield of 42.82% and good photostability, which made them promising candidates in the fields of sensors, drug delivery and biomedical imaging.

## Nanotubes

In 2011, Li et al fabricated graphdiyne nanotube (GDYNT) arrays through an anodic aluminum oxide template technique catalyzed by Cu-pyridine complex (Figure 1).<sup>24</sup> The tubular GDY exhibited a smooth surface with a diameter of ~200 and a wall thickness of ~40nm. After annealing treatment at 650°C for 6h, GDYNT's wall thickness decreased to 15 nm, a third of the origin, which helped enhance field emission property. GDYNTs' field and threshold field decreased to 4.20 and 8.83 V/ $\mu\text{m}$ , respectively, with more field emission stability than that of carbon nanotubes. In 2015, Jalili et al demonstrated that

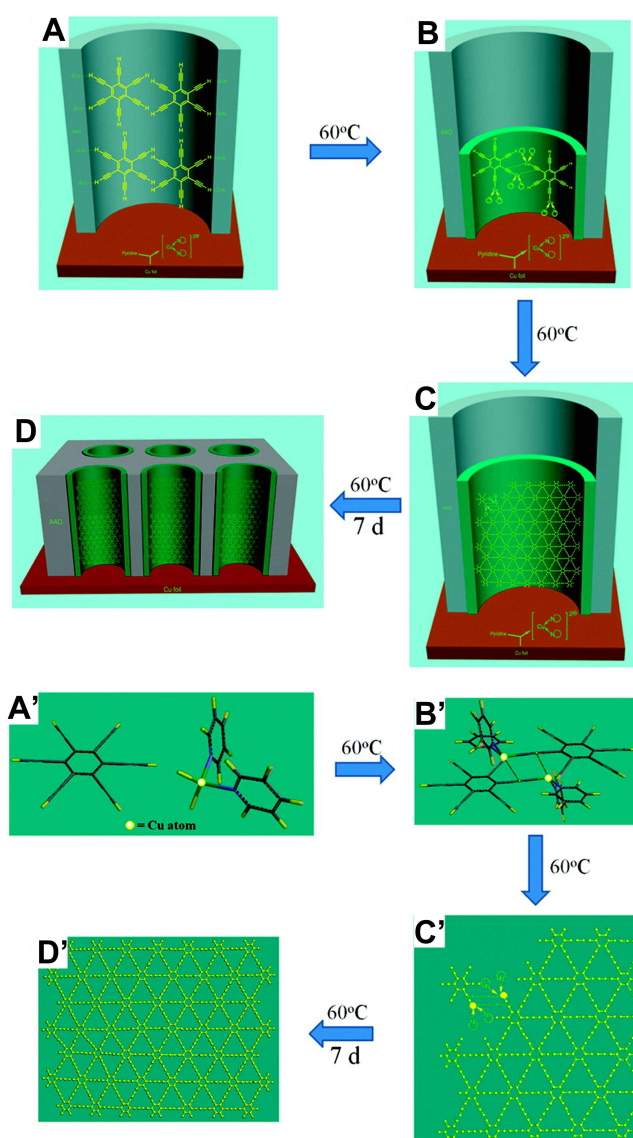


**Figure 1** The process (A–D) and proposed mechanism (A'–D') to fabricate GDNT arrays.<sup>24</sup>

**Notes:** Reproduced from Li G, Li Y, Qian X, et al. Construction of tubular molecule aggregations of graphdiyne for highly efficient field emission. *J Phys Chem C*. 2011;115(6):2611–2615. Copyright 2011, American Chemical Society.<sup>24</sup>

GDYNTs exhibit higher charge carrier mobility than both graphdiyne sheets and carbon nanotubes theoretically.<sup>25</sup> In 2016, Shohany et al found that pores uniformly distribute on the sidewall of GDYNT, which could simplify the electron transport.<sup>26</sup> By the combination of density functional theory (DFT) and non-equilibrium Green's function method, they confirmed that all the nanotubes display semi-conducting behavior and the energy bandgap negatively correlates with nanotube diameter. In 2016, Pari et al found that zigzag GDYNT is more stable in structure compared to their armchair counterparts of the same size, which is expected to have a higher electron and hole mobility.<sup>27</sup>

## Nanowires

In 2012, Qian et al prepared graphdiyne nanowires (GDNWs) with high-quality defect-free surface via a modified VLS mechanism, in which ZnO was reduced to Zn by graphdiyne.<sup>28</sup> In the growth process, graphdiyne kept stable at 750°C and the graphdiyne segments of low molecular weight would become vapor, which later deposited on the substrate of ZnO nanorod arrays (Figure 2). In 2014, Cirera et al realized preparation of extended GDNWs with atomical precision via a surface-assisted covalent mechanism (Figure 3).<sup>29</sup> By employing Ag (877) vicinal surface, the terminal alkyne reactants were guided by its regular step-terrace topology, which inhibited unwanted branching side reactions and thus enhanced chemoselectivity of the targeted linear homocoupling. Later in 2018, Klappenberger et al obtained carbonitrile-functionalized GDNWs by similar on-surface strategy, which not only enabled selective alkyne homocoupling reaction but also ensured the double-stranded assemblies temperature stability.<sup>30</sup>

## Nanoribbons

In 2020, Zhou et al first proposed bottom-up synthesis of GDY nanoribbons through selective stepwise coupling reaction of ethynyl groups.<sup>31</sup> Though there have been many theoretical investigations on electronic structures and properties in graphdiyne-based nanoribbons (GDYNRs), how to produce GDYNRs with well-defined edges and widths remains a significant challenge.<sup>32,33</sup> This synthetic strategy followed two steps (Figure 4). First, ethynyl groups in the center of the monomer polymerize ensure the planar growth. Next, edge-on Glaser–Hay coupling reaction of ethynyl groups is obtained from liquid/liquid interfacial reaction. The prepared GDYNRs are composed of benzenes and butadiyne rhomboids with well-defined edges and nanometer widths. This controllable synthesis strategy constructed GDYNRs with high chemical precision and made them able to have different width and edge structures and add functional groups at the outer edge. Due to the high tendency to be interwoven into nanotextiles, self-assembled ribbons could be applied as a protective coating for lithium electrodes in Li-ion batteries.

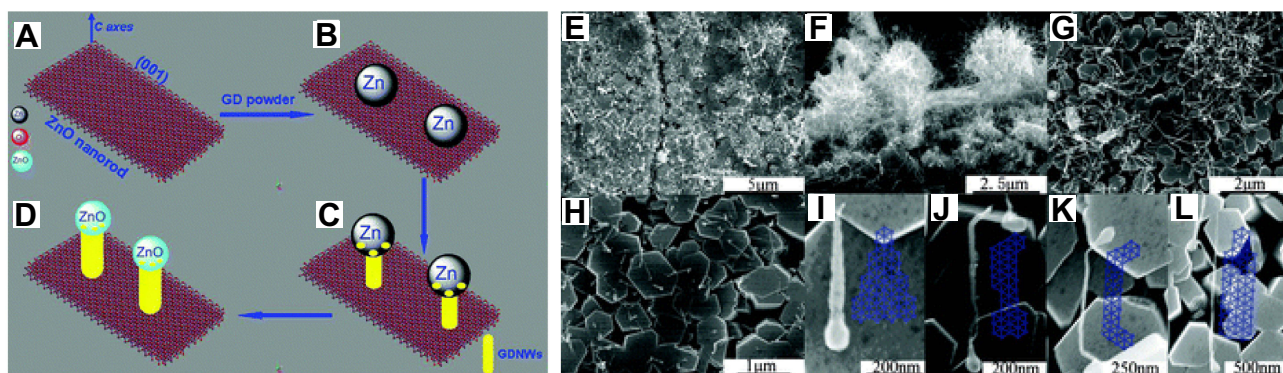


**Figure 2** Schematic illustration of the VLS process in the growth of GDNWs (A–D). SEM images of GDNWs: (E–H) low-magnification images of GDNWs grown in different areas. (I–L) High-magnification images of single GDNWs with different lengths and diameters: (I) ~550 nm in length, ~46 nm in diameter; (J) ~780 nm in length, ~23 nm in diameter; (K) ~1070 nm in length, ~20 nm in diameter; (L) ~1700 nm in length, ~33 nm in diameter.<sup>28</sup>

**Notes:** Used with permission of Royal Society of Chemistry, Qian X, Ning Z, Li Y, et al. Construction of graphdiyne nanowires with high-conductivity and mobility. Dalton Trans. 2012;41(3):730–733; permission conveyed through Copyright Clearance Centre, Inc.<sup>28</sup>



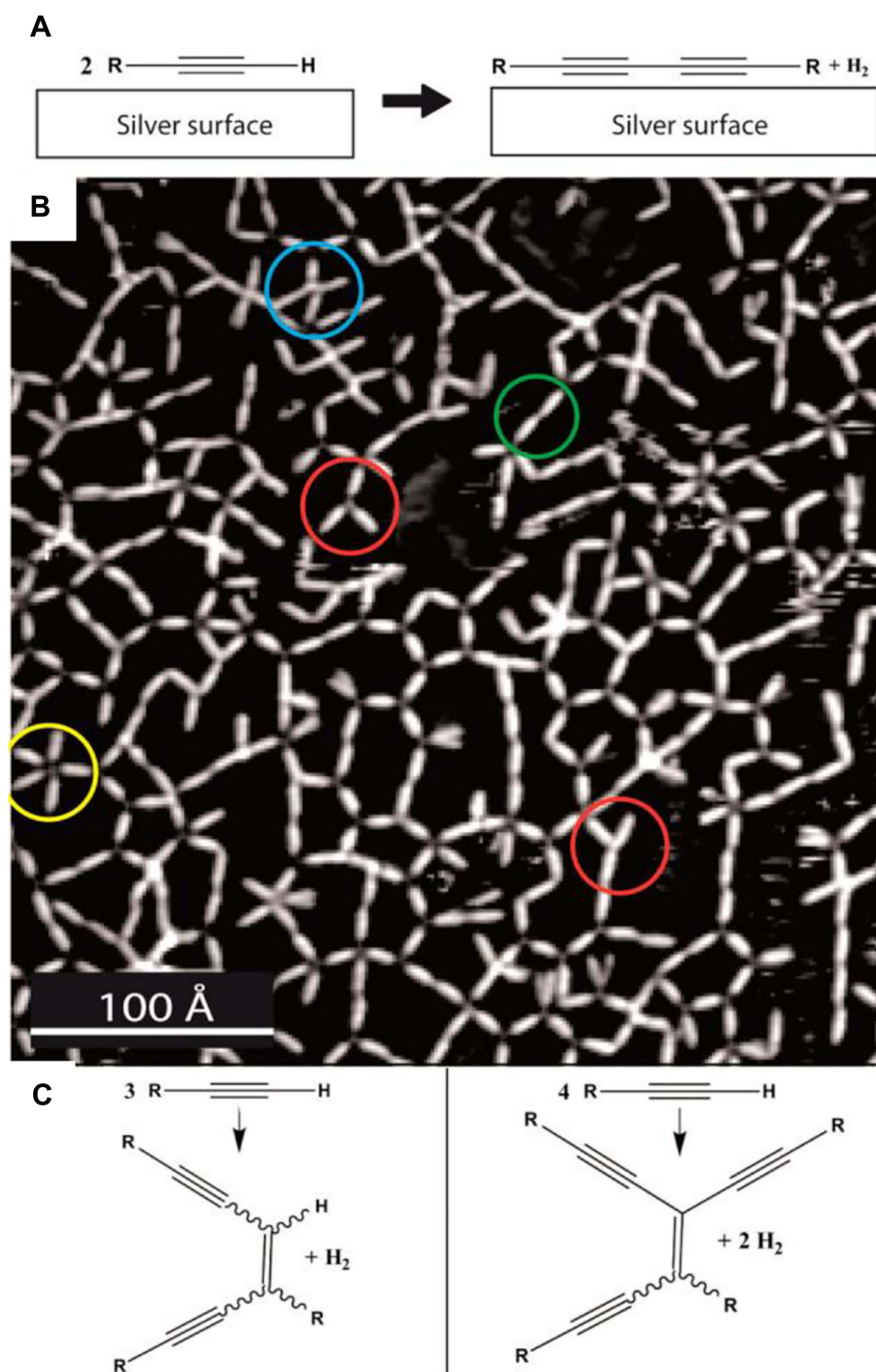


**Figure 3** (A) Schematic representation of the targeted linear covalent homocoupling reaction of the terminal acetylenic compounds with the Ag(111) surface as a catalyst. (B) STM image of a polymerized, irregular porous network fabricated by annealing I on the Ag(111) substrate to 400 K. Reaction products resulting from covalent coupling of two, three, four, or even five monomers are highlighted in green, red, blue, and yellow, respectively. (C) Examples of side reactions involving three and four reacting monomers.<sup>29</sup> **Notes:** Reproduced from Cirera B, Zhang YQ, Björk J, et al. Synthesis of extended graphdiyne wires by vicinal surface templating. *Nano Lett.* 2014;14(4):1891–1897. Copyright 2014, American Chemical Society.<sup>29</sup>

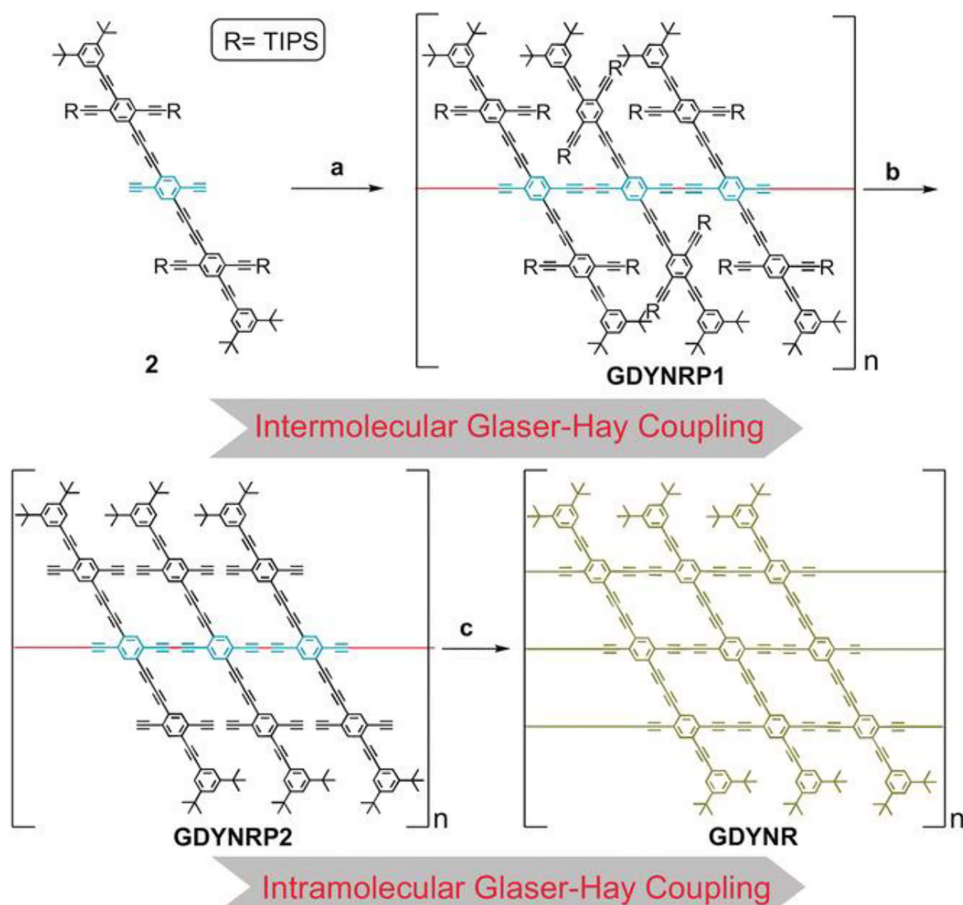


**Figure 4** Stepwise intermolecular and intramolecular Glaser-Hay coupling reaction for GDYNR. a) CuCl, TMEDA, acetone/THF, RT; b) TBAF, THF, RT; c) interfacial reaction, Cu(OAc)<sub>2</sub> and pyridine in H<sub>2</sub>O, GDYNRP2 in CH<sub>2</sub>Cl<sub>2</sub>, RT.<sup>31</sup>

**Abbreviations:** TIPS, triisopropylsilyl; TBAF, tetrabutylammonium fluoride; RT, room temperature.

**Notes:** Reproduced from Zhou W, Shen H, Zeng Y, et al. Controllable synthesis of graphdiyne nanoribbons. *Angew Chem Int Ed.* 2020;59(12):4908–4913. Copyright 2020, Wiley and Sons.<sup>31</sup>

## Nanowalls

In 2015, Zhou et al synthesized GDY nanowalls with copper plate as substrate and hexaethynylbenzene (HEB) as monomer (Figure 5).<sup>34</sup> In the presence of the catalytic amount of a nitrogen ligand N,N,N',N'-tetramethylethylenediamine (TMEDA), copper converted to Cu ions easily forming the controllable reaction sites. GDY nanowalls grew vertically and uniformly on the substrate rapidly when the ratio of solvent, pyridine and TMEDA is proper. When an exfoliated GDY sample was transferred on Si/SiO<sub>2</sub> substrate, the walls showed layer structure with thickness ranging from several to dozens of nanometers. These GDY nanowalls showed high crystallization and excellent and stable field-emission properties. The same reaction was utilized to fabricate GDY nanowalls on copper foam which acted as robust 3D porous substrate and catalyst.<sup>19</sup> While the abovementioned methods are limited by the catalyst, Gao developed a copper envelope catalysis strategy to prepare GDY nanowalls on arbitrary substrates in 2017.<sup>35</sup> The copper-pyridine complex diffused from the copper envelope to target substrates, ensuring sufficient concentration of catalyst and thus in situ growth of GDY. The author adopted this simple design to fabricate GDY nanowalls on a BiVO<sub>4</sub> electrode, which enhanced the photoelectrochemical performance of BiVO<sub>4</sub> greatly. The photoelectrochemical (PEC) performance of GDY nanowalls was demonstrated in the introduction to the Si-based PEC system which exhibited enhanced water splitting performance.<sup>36</sup>

## Nanosheets

In 2017, Matsuoka proposed a bottom-up method to generate multilayer GDY nanosheets (GDNSs) with verified in-plane periodicity at a liquid-liquid interface (Figure 6).<sup>37</sup> GDY nanosheets grew between the upper aqueous layer

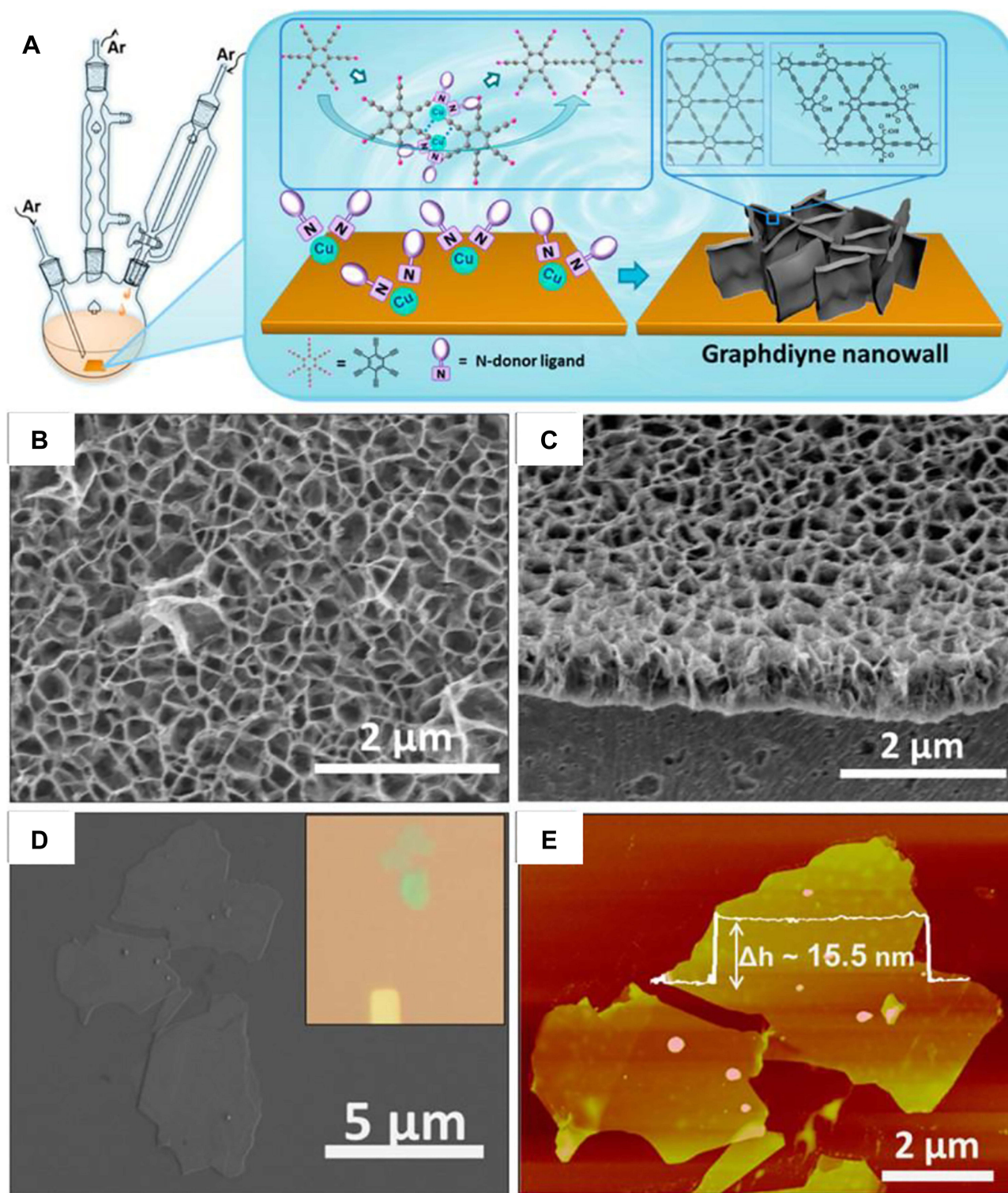


**Figure 5** (A) Schematic illustration of the experimental setup. SEM images of graphdiyne nanowalls on Cu substrate: (B) top view, (C) cross-sectional view. (D) SEM image and OM image (inset) of an exfoliated sample. (E) AFM image of an exfoliated sample on Si/SiO<sub>2</sub> substrate. The height profile is taken along the white line, representing a 15.5 nm-thick film.<sup>34</sup> **Notes:** Reproduced from Zhou J, Gao X, Liu R, et al. Synthesis of graphdiyne nanowalls using acetylenic coupling reaction. *J Am Chem Soc.* 2015;137(24):7596–7599. Copyright 2015, American Chemical Society.<sup>34</sup>

containing a copper catalyst and the lower organic layer dissolving HEB and became a framework with 24 nm thickness and a step of 6 nm at the edge. Additionally, they successfully employed a gas-liquid interfacial strategy to achieve single-crystalline GDY nanosheets, which had narrow distributions of the thickness (as thin as 3nm) and



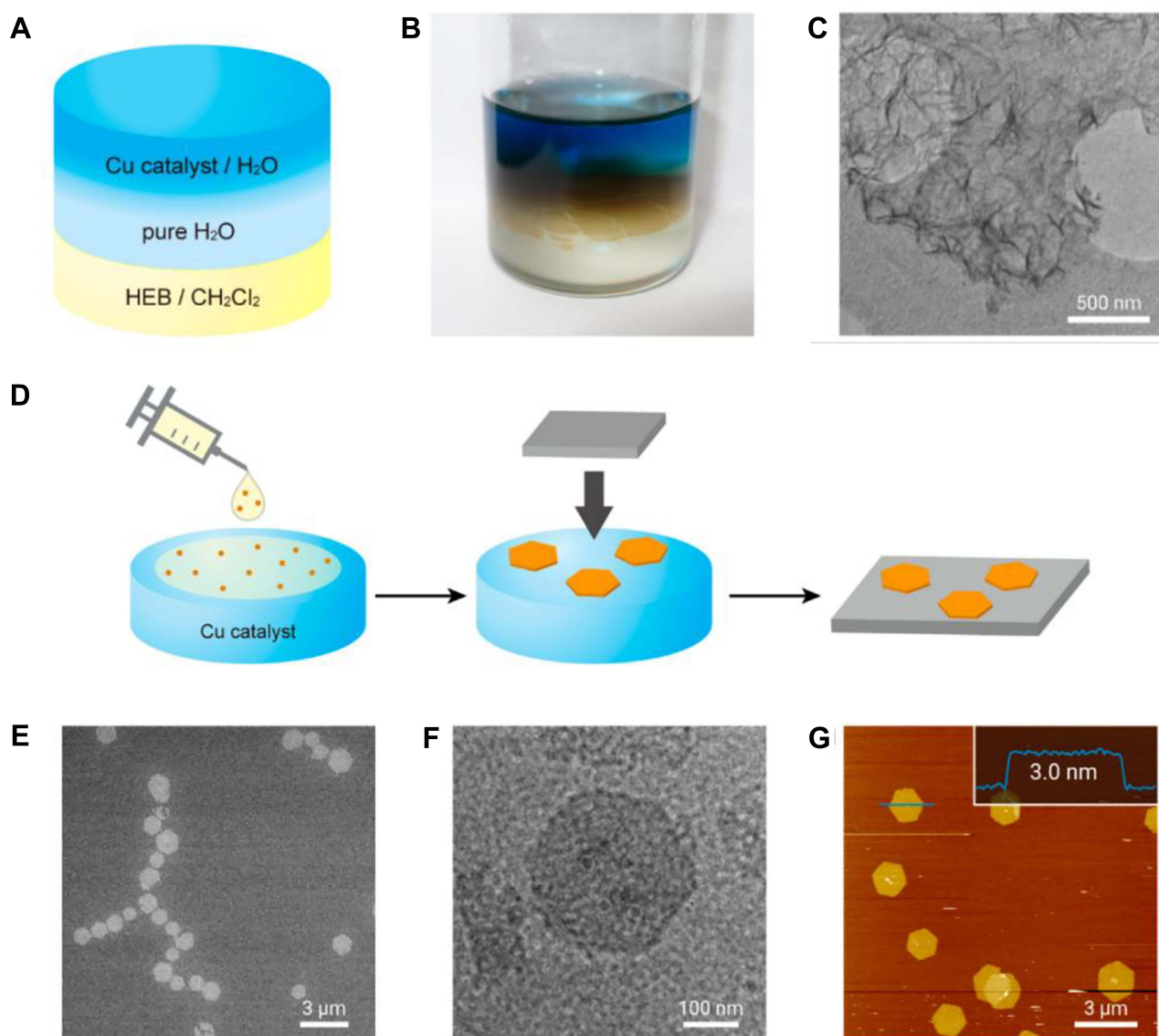


**Figure 6** Schematic illustration (A) and photograph (B) of the liquid–liquid interfacial synthetic procedure. (C) TEM of a holey elastic carbon matrix. (D) Schematic illustration of the gas–liquid interfacial synthesis and transfer process. (E) SEM of HMDS/Si (100). (F) TEM of an elastic carbon grid. (G) AFM topographic image of HMDS/Si (100) and its cross-sectional analysis along the blue line.<sup>37</sup>

**Notes:** Reproduced from Matsuoka R, Sakamoto R, Hoshiko K, et al. Crystalline graphdiyne nanosheets produced at a gas/liquid or liquid/liquid interface. *J Am Chem Soc.* 2017;139(8):3145–3152. Copyright 2017, American Chemistry Society.<sup>37</sup>

lateral size (1.5  $\mu\text{m}$ ). This well-defined regular hexagonal GDY had good crystallinity and a much lower oxygenic defect level. In 2018, Shang et al realized large-scale production of ultrathin GDYNSs via free-standing Cu nanowire. Since Cu acted as a substrate as well as a strong catalyst for GDY growth, the nanostructure and quality of GDY could be controlled (Figure 7).<sup>17</sup> The GDYNSs could be used as Li-ion battery anode due to their high capacity and rate performance for storing  $\text{Li}^+$ . They then succeeded in editing the N-content, micropores and surface area of GDY through solvent- and metal-catalyst-free method in the air at 120°C.<sup>38</sup> In 2019, Pan et al utilized the controllability of liquid–liquid interfacial synthesis to dope GDY with a different number of N atoms through monomer design, which could modulate its wettability, pore size and electronic property.<sup>10</sup> In 2021, Navaee et al prepared GDY nanosheets at cathode of bipolar via bipolar electrochemistry method.<sup>39</sup> The coupling reaction realized a high efficient yield of GDY nanosheets on the copper bipolar electrode in a 2:1 ethanol and acetonitrile solvent.



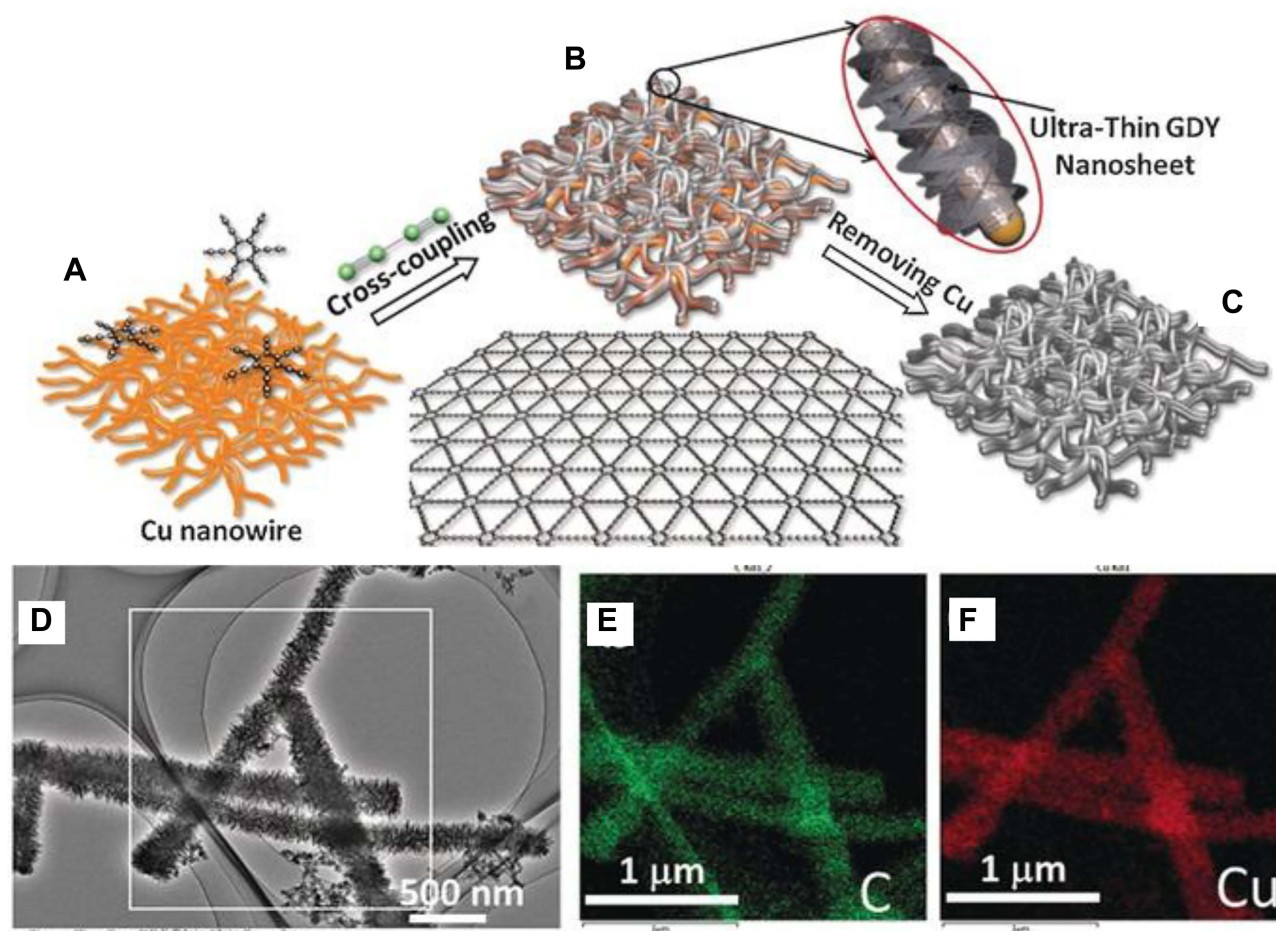


**Figure 7 (A-C)** Representation of the synthesis of GDY on CuNW paper. TEM (D) and elemental mapping (E and F) of GDY nanosheets with CuNWs.<sup>17</sup>

**Notes:** Reproduced from Shang H, Zuo Z, Li L, et al. Ultrathin graphdiyne nanosheets grown in situ on copper nanowires and their performance as lithium-ion battery anodes. *Angew Chem Int Ed.* 2018;57(3):774-778. Copyright 2018, John Wiley and sons.<sup>17</sup>

## Ordered Stripe Arrays

In 2017, Wang et al proposed a wettability-facilitated strategy that addressed the challenge of synthesizing GDY with a precise pattern.<sup>40</sup> It utilized superhydrophilic grooved templates to restrict the spacing of the reaction process at the microscale for the in situ fabrication of GDY (Figure 8). The size of GDY stripe arrays was modulated by the silicon substrate size and the thickness could be regulated by the concentration of hexaethylbenzene monomers. The author proved that GDY stripe array-based stretchable sensor could detect the finger joint motion and was promising for other optoelectronic applications.

## Nanospheres

In 2022, Yu et al produced GDY nanospheres confined in the mesoporous channels of Pd/mSiO<sub>2</sub> by a defined explosion approach (Figure 9).<sup>41</sup> First, HEB was absorbed in mesoporous Pd/SiO<sub>2</sub> in ethyl acetate solution. After heating HEB at 120°C in the air, cross-coupling reaction occurred quickly and thus obtained GDY@Pd/mSiO<sub>2</sub> composite. GDY nanospheres impressively enhanced hydrogenation rates via wettability and electronic modifier. Nanospheres with large surface area and high reactivity exhibit great potential for targeted delivery of drugs and the application of GDY nanospheres remains to be explored.

## Biomedical Application

The sp<sup>2</sup>- and sp-hybridized flat framework endows GDY with highly conjugated surface, adjustable electronic properties and uniformly distributed nanopores has attracted the attention of many researchers. The development

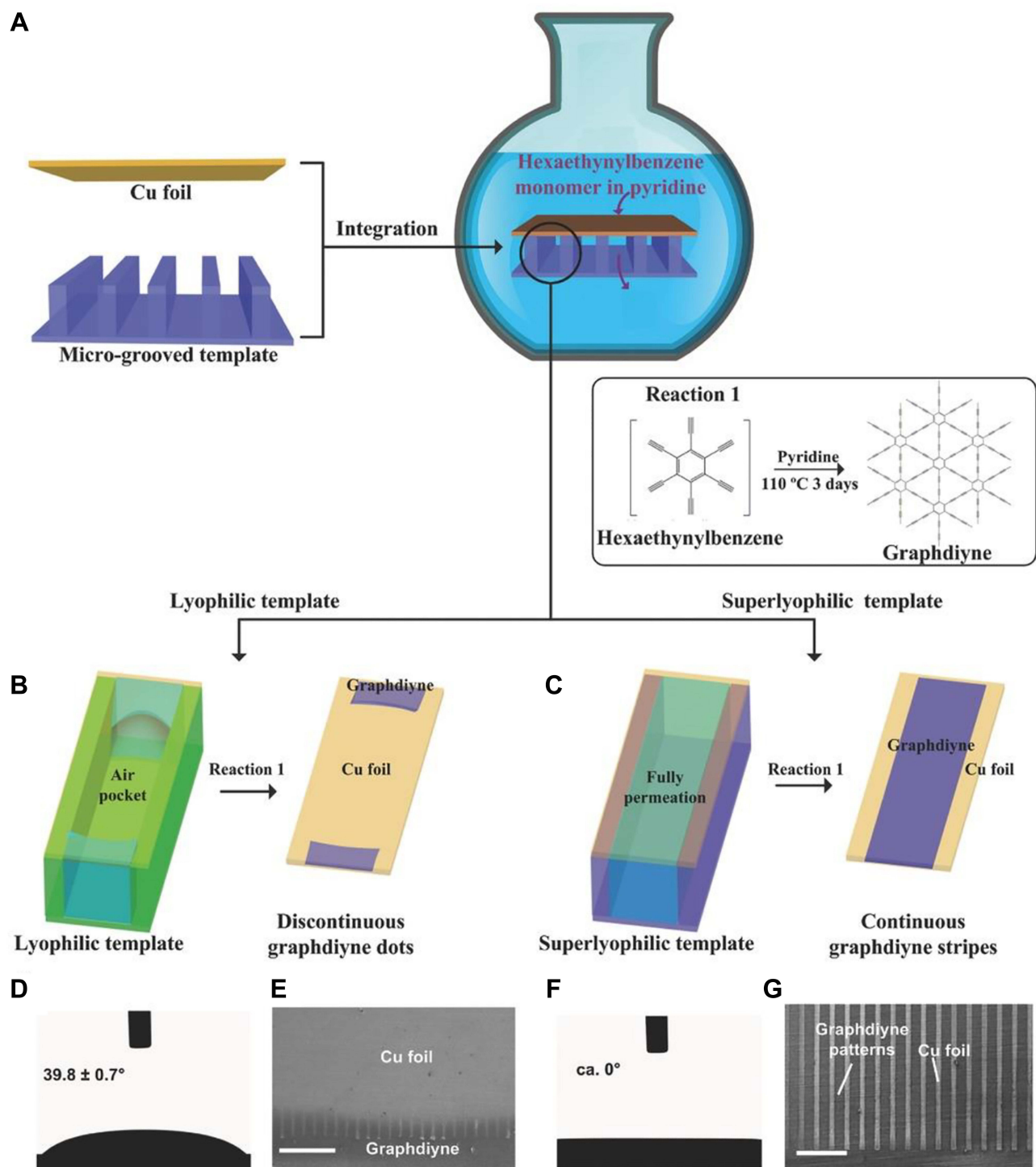


**Figure 8 (A–C)** Schematic illustration of the in situ synthesis of graphdiyne linear patterns. The contact angles of pyridine ( $\gamma = 39.82 \text{ mN}\cdot\text{m}^{-1}$ ) droplet on the **(D)** lyophilic and **(F)** superlyophilic grooved templates. **(E and G)** Corresponding scanning electron microscopy images of graphdiyne growth upon the copper foils.<sup>40</sup>  
**Notes:** Reproduced from Wang SS, Liu HB, Kan XN, et al. Superlyophilicity-facilitated synthesis reaction at the microscale: ordered graphdiyne stripe arrays. *Small*. 2017;13(4):1602265. Copyright 2017 John Wiley and Sons.<sup>40</sup>

of synthetic approaches for GDY with many nanostructures has contributed to improving their electronic and mechanical properties and thus fulfilling their potential in biological and medical fields. This part presents the use and advantages of GDY-based materials in various biomedical applications of biosensing, cancer theranostic platform, radiation protection and tissue engineering and their advantages are summarized in [Table 2](#).

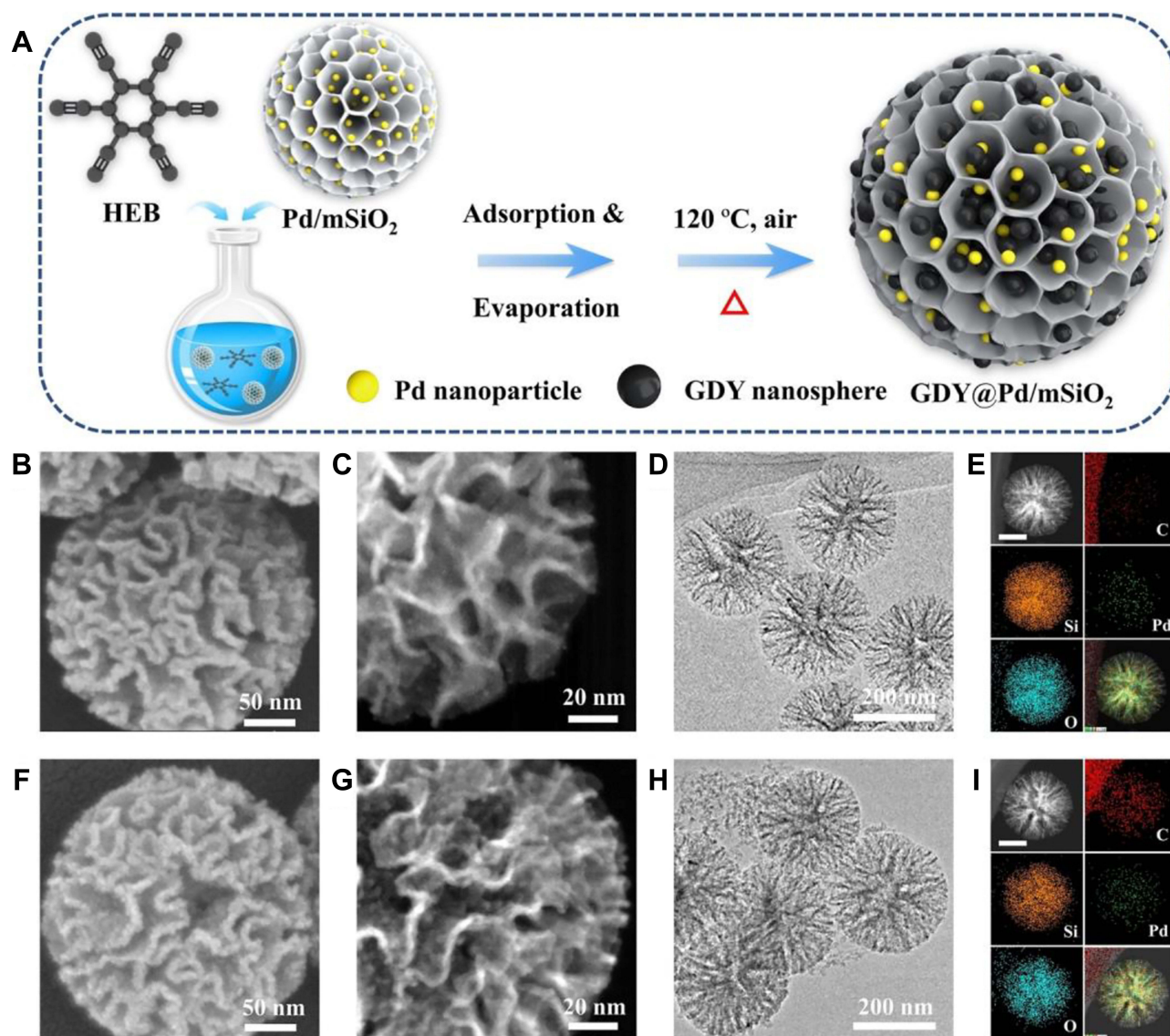


**Figure 9** (A) Schematic illustration of the synthesis procedures for GDY@Pd/mSiO<sub>2</sub>; (B) SEM, (C) SEI-STEM, (D) TEM, (E) EDS mapping images of Pd/mSiO<sub>2</sub>; (F) SEM, (G) SEI-STEM, (H) TEM, (I) EDS mapping images of 20 GDY@Pd/mSiO<sub>2</sub>. Scale bars 100 nm (E and I).<sup>41</sup>

**Notes:** Reproduced from Yu J, Chen W, Li K, et al. Graphdiyne nanospheres as a wettability and electron modifier for enhanced hydrogenation catalysis. *Angew Chem Int Ed.* 2022;61(34):e202207255. Copyright 2022, John Wiley and Sons.<sup>41</sup>

## Biosensing DNA

Low-dimension nanomaterials have been used as fluorescent sensing platforms for DNA detection due to their different affinities towards DNA probes and high fluorescence quenching efficiency.<sup>42,43</sup> The biosensors offer stronger binding with single-stranded DNA (ssDNA) than double-stranded DNA (dsDNA) via van der Waals force between adjacent layers and covalent bonding. Such fluorescent-quenching property is highly sensitive and selective through fluorescence resonance energy transfer (FRET) or photo-induced electron transfer (PET).<sup>44</sup> When the probe forms hybridization with its complementary target DNA, the interaction between platform and nucleobases weaken and dye-labeled ssDNA release, which result in fluorescence restoration.

In 2016, graphdiyne nanosheets and its oxide labeled with 5-carboxyfluorescein was first applied as nanoquencher for sensing biomolecules such as DNA, which outperform those based on carbon-based nanostructures.<sup>45</sup> The strong fluorescence quenching ability of GDY was ascribed to Van der Waals force and  $\pi$ - $\pi$  stacking interaction between



**Table 2** Advantages of GDY-based nanomaterials use in biomedical applications

		Advantages	Ref.
Biosensing	DNA	More sensitive than other carbon-based nanostructures	[45]
	Glucose	Higher sensitivity and shorter detection time than other colorimetric method-based sensors	[49]
	Amino acids	Higher absorption energy than that on graphene	[51]
	Fe <sup>3+</sup>	Much more sensitive than most of the other fluorescent sensors	[53]
Cancer theranostic platform			
Diagnosis	MicroRNA detection	Enhanced PEC performance	[66]
	MI	Excitation- and pH-dependent fluorescence emission, as well as superior photostability	[52]
	PAI	Outstanding photoacoustic stability	[55]
Therapy	Drug delivery	Higher loading of anticancer drugs than other 2D-based micromotors	[90]
	PTT	More efficient photothermal conversion efficiency than classic PTT agents	[93,94]
	PDT	High affinity for transition metals	[95]
Radiation protection		Stronger radical-scavenging ability than graphene oxide	[106]
Tissue engineering	Antibacterial	Broad-spectrum antibacterial activity	[111,114]
	Bone repair	Improved hydrophilicity and biocompatibility	[112]

GDY and ssDNA. Hydroxyl and carboxyl groups of graphdiyne oxide (GDYO) made it exhibit stronger quenching ability than GDY due to various interactions with nucleobases and improving dispersity in water. In 2017, Parvin et al developed few-layer GDY nanosheets for multiplexed DNA real-time detection which possesses high efficiency and remarkable sensitivity with a limit of detection of  $25 \times 10^{-12}$  M (Figure 10).<sup>46</sup> The author carried out DFT to confirm the stronger interaction of GDY with 6-carboxyfluorescein than that of graphene. A pair of  $\pi$  bonds in the triple bond of GDY contributes to its distinguished adsorption strength ( $344.48 \text{ kJ mol}^{-1}$ ) and shorter interaction distance (3.583 Å), facilitating enhanced fluorescence quenching. All of these made GDY-based biosensors outperformed GO and MoS<sub>2</sub> nanomaterial-based sensors. Recently in 2019, the thinnest GDY nanosheet (only ~0.9 nm) was exfoliated. A sensing

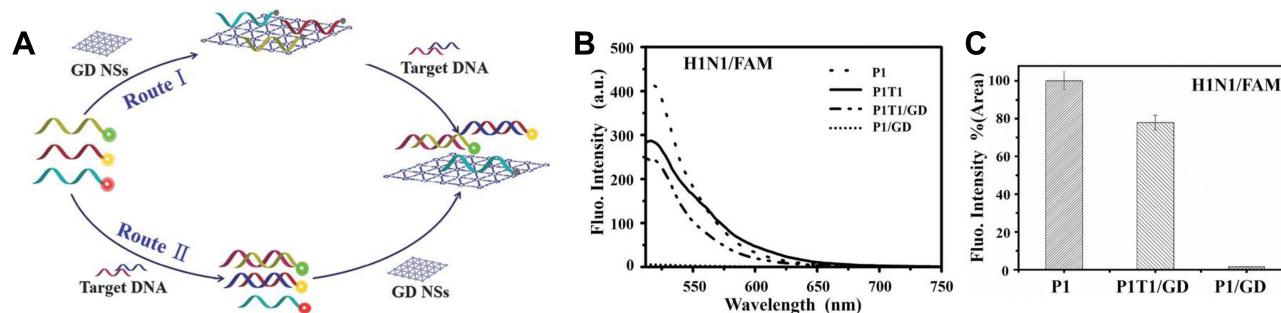


**Figure 10** (A) Scheme for the GD-based multiplexed DNA detection through different routes. Route I: dye-labeled ssDNA with different fluorescence was first mixed with GD NSs, resulting in complete quenching of the dyes. Then, in the presence of the target DNA (T1, ruby; T2, blue), the forming of dsDNA makes the release of dye-labeled DNA from the surface of GD NSs result in fluorescence recovery, finishing the detection. Route II: dye-labeled ssDNA was first mixed with target DNA, then GD NSs were added for detection. (B) Fluorescence spectra of FAM-labeled H1N1 ssDNA (P1:H1N1-FAM). (C) Fluorescence intensity of ssDNA and dsDNA probes with and without GD.<sup>46</sup>

**Notes:** Reproduced from Parvin N, Jin Q, Wei Y, et al. Few-layer graphdiyne nanosheets applied for multiplexed real-time DNA detection. *Adv Mater.* 2017;29(18):1606755. Copyright 2017, John Wiley and Sons.<sup>46</sup>



platform based on it was applied for detecting mycobacterium tuberculosis and its drug resistance genes sensitively and selectively.<sup>47</sup>

## Glucose

Glucose is a significant indicator of human bodies relating to many endocrine diseases, the concentration of which is needed to be monitored. Conventional methods of glucose detection include enzyme-based coloring method, electrochemical detection and HPLC method, among which the enzymatic method is most widely used for its adequate sensitivity.<sup>48</sup> Conventional glucose detection involves two procedures. First, glucose is oxidized by oxygen to produce hydrogen peroxide catalyzed by glucose oxidase. Second, the as-produced hydrogen peroxide oxidizes chromogenic agents with color reaction. While ferrous ion ( $\text{Fe}^{2+}$ ) is significant in the enzymatic catalytic reaction, it tends to be oxidized into ferric ion ( $\text{Fe}^{3+}$ ). In 2019, Liu et al synthesized GDY with dual-enzymatic activity via immobilizing ferrous ion and glucose oxidase.<sup>49</sup> This GDY-based glucose sensor combining peroxidase activity of  $\text{Fe}^{2+}$  with glucose oxidase activity succeeded in merging two steps into one step (Figure 11). Compared to graphene, GDY exhibited stronger adsorption for ferrous ion due to lower adsorption energy resulted from its sp<sup>2</sup>-hybridized carbon atoms. Meanwhile, GDY helped retain high catalytic activity of  $\text{Fe}^{2+}$  as well as glucose oxidase (GOx). Fe-GDY/GOx displayed higher sensitivity and shorter detection time than other glucose detection sensors and the feasibility of this method on blood glucose detection was verified in rat model. In 2021, Zhu et al synthesized hemin/GDYO nanocomposite-based colorimetric method for the quantitative determination of glucose with a detection limit of 38 $\mu\text{M}$ .<sup>50</sup> Compared with GDY, better dispersion made GDYO an outstanding absorption substrate for iron porphyrin hemin. After combination with hemin, the nanocomposite exhibited superior peroxidase-like activity and affinity for glucose.

## Amino Acids

In 2015, Chen et al investigated the interaction between GDY and amino acids by theoretic study, revealing GDY as a promising biosensor for amino acids.<sup>51</sup> Attributed to dispersion interactions and electrostatic polarization,

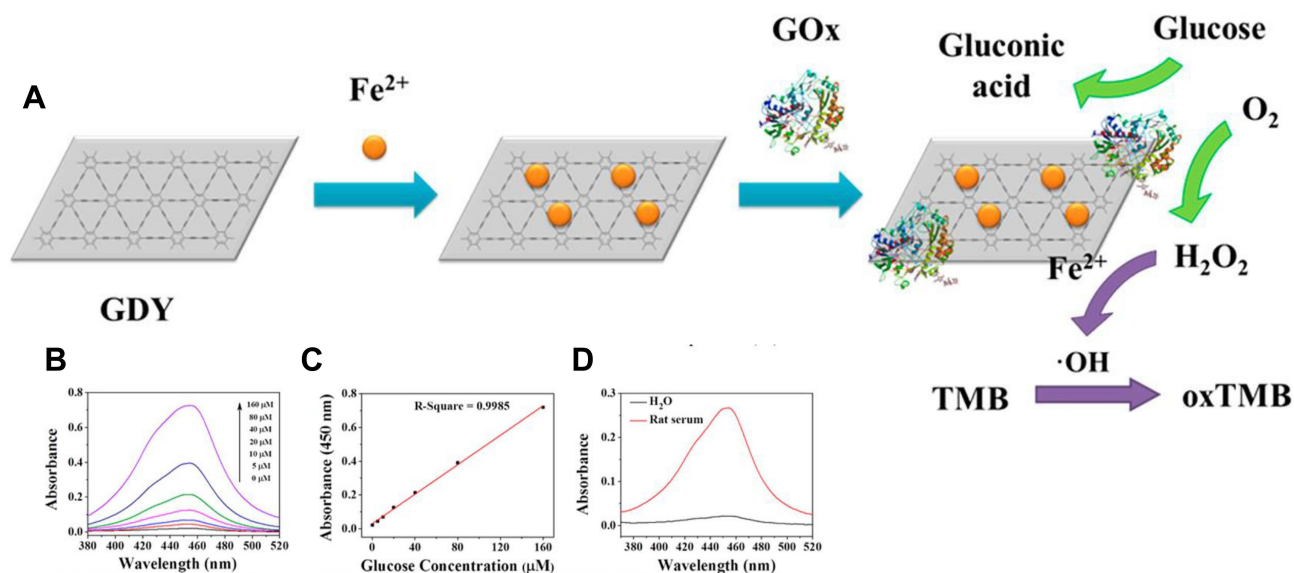


**Figure 11 (A)** Schematic Illustration to show the preparation of Fe-GDY/GOx and mechanism for glucose detection. **(B)** UV-vis spectra of buffer solution containing 400  $\mu\text{M}$  TMB, 80  $\mu\text{g/mL}$  Fe-GDY/GOx, and glucose with different concentrations after 25 min reaction; **(C)** linear calibration plot for glucose using Fe-GDY/GOx; **(D)** UV-vis spectra of buffer solution containing 400  $\mu\text{M}$  TMB, 80  $\mu\text{g/mL}$  Fe-GDY/GOx, and diluted rat serum (red line) or water (black line).<sup>49</sup>  
**Notes:** Reproduced from Liu J, Shen X, Baimanov D, et al. Immobilized ferrous ion and glucose oxidase on graphdiyne and its application on one-step glucose detection. ACS Appl Mater Interfaces. 2019;11(3):2647–2654. Copyright 2019, American Chemistry Society.<sup>49</sup>

GDY has higher absorption energy than graphene. Moreover, the characteristically depressing photon absorption peaks of graphdiyne–amino acid systems offers a positive approach to the electronic detection of amino acids.

### Fe<sup>3+</sup>

Fe<sup>3+</sup>, an ionic form of the iron element in blood, may affects human health when it is excessive. GDY with optical properties is prospective as fluorescent materials and in 2020 graphdiyne oxide quantum dots (GDYO-QDs) were firstly prepared for subsequent detection of ferric ion and ascorbic acid (Figure 12).<sup>52,53</sup> The fluorescence of GDYO-QDs can be efficiently quenched by Fe<sup>3+</sup> attributed to the synergistic effect of inner filter effect and photo-induced electron transfer. This nanosensor for Fe<sup>3+</sup> with a limit of detection as low as 95 nmol L<sup>-1</sup> and a linear range of 0.25–200 μmol L<sup>-1</sup> exhibited more sensitivity than most of the other fluorescent sensors. About 85% fluorescence could be recovered by ascorbic acid via reducing Fe<sup>2+</sup> to Fe<sup>3+</sup>. The authors demonstrated the off/on sensor could be recycled at least three times with high anti-interference and further verified its function in fetal bovine serum samples, and further work is to improve the quantum yields of GDYO-QDs.

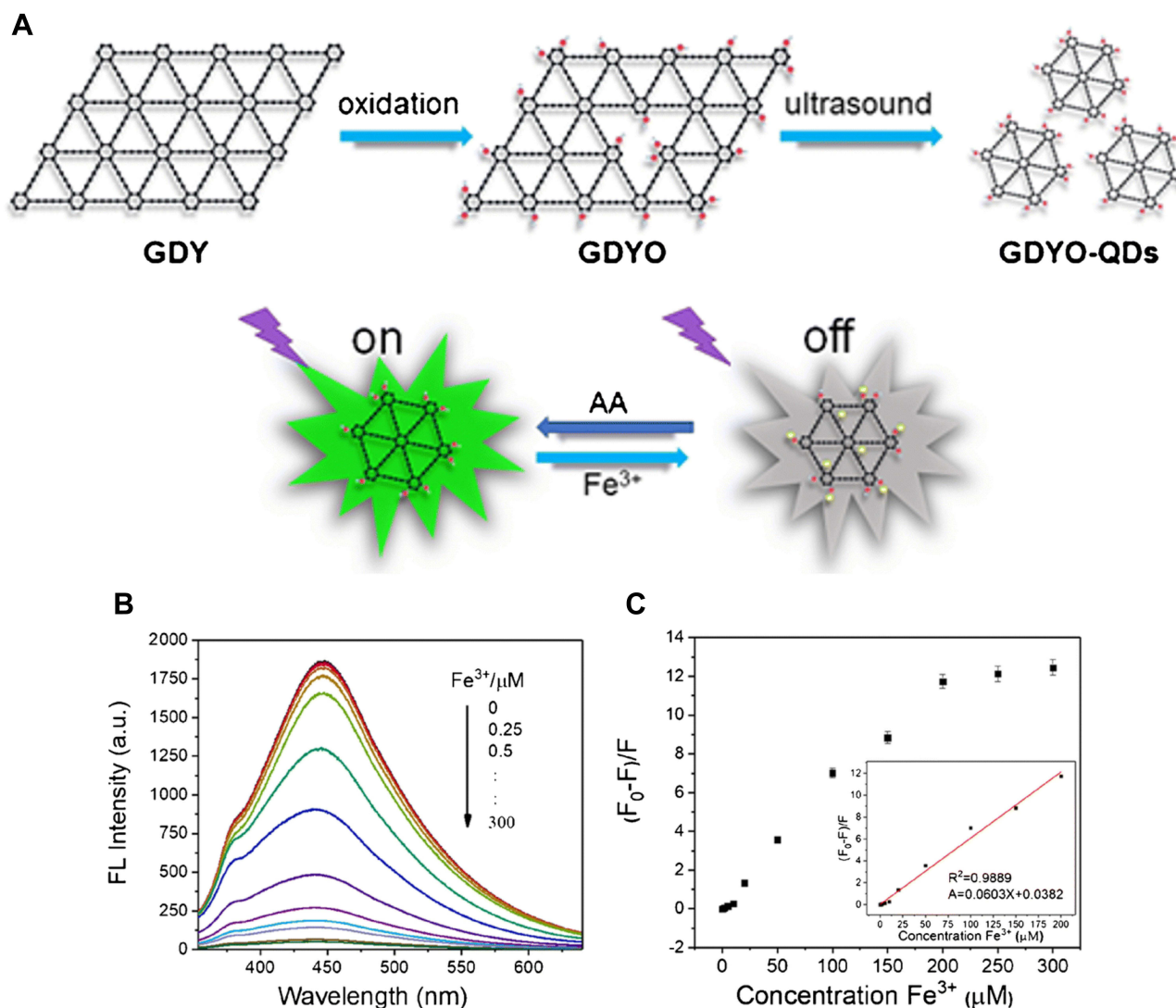


**Figure 12** (A) Synthesis of GDYO-QDs and fluorescence detection of Fe<sup>3+</sup> and AA. (B) Fluorescence spectra of GDYO-QDs for the detection of different concentrations of Fe<sup>3+</sup> (from top to bottom: 0–300 μmol L<sup>-1</sup>). (C) Calibration curve of (F<sub>0</sub>-F)/F versus Fe<sup>3+</sup> concentration. The inset is the calibration curve of (F<sub>0</sub>-F)/F and low-concentration Fe<sup>3+</sup> (0.25–200 μmol L<sup>-1</sup>).<sup>53</sup>

**Notes:** Reproduced from Bai Q, Zhang C, Li L, et al. Subsequent monitoring of ferric ion and ascorbic acid using graphdiyne quantum dots-based optical sensors. *Microchim Acta*. 2020;187(12):657. Copyright © 2020, Springer-Verlag GmbH Austria, part of Springer Nature.<sup>53</sup>

## Cancer Theranostic Platform

### Diagnosis

Cancer imaging is a powerful tool in early detection and precise diagnosis of cancer. Magnetic resonance imaging (MRI), computed tomography (CT) and positron emission computed tomography (PET) are common techniques in clinical application. Whereas, these methodologies have some limitations (eg, lack of specificity and high irrational burden) and new imaging techniques are in need.<sup>54,55</sup>

Photoelectrochemical detecting technology has been fully elucidated to be a sensitive, simple and cheap tool.<sup>56–58</sup> The underlying mechanism is based on monitoring a specific combination of photoactive biosensor materials and target molecules, which brings photocurrent/photopotential changes with reduced background signal.<sup>59,60</sup> Inorganic semiconductors, hybrid metal/semiconductor nanoparticle and organic small molecules have been applied extensively due to their excellent PEC properties.<sup>61–63</sup> In 2016, Li groups demonstrated that GDY with an appearance of a cross-linked nanowall could produce hole–electron pairs, which was beneficial for hole transfer and photocurrent enhancement.<sup>64</sup> In 2019, Zhang et al introduced GDY nanowalls into the Si-based PEC system, which improved the saturated photocurrent density up to  $39.1 \text{ mA}\cdot\text{cm}^{-2}$ .<sup>36</sup> Experiments above verified GDY as a promising photoactive material candidate with high photoelectric conversion efficiency. In 2019, Li et al synthesized GDY loaded with gold nanoparticles (AuNPs) for microRNA detection.<sup>65</sup> The surface plasmon resonance (SPR) effect of AuNPs helps GDY obtain strong photocurrent output. When the mass ratio of GDY to tetrachloroauric acid was 1:2.5, AuNPs distributed uniformly and their shapes were relatively regular, which was beneficial for enhancing PEC response. The results showed outstanding PEC property for microRNA let-7a, a significant marker of malignant tumors.<sup>66</sup> With the advancement of GDY, PEC biosensors for cancer classification will continue to evolve.

Fluorescence molecular imaging (MI) techniques are specific and noninvasive tools in cancer diagnosis via detecting complex spatiotemporal interplay of biomolecules. While low photobleaching thresholds and weak solubility limit the application of conventional fluorescent proteins and dyes,<sup>67</sup> the unique optical properties of semiconductor quantum dots (QDs) make them an appealing supplement. Other appealing optical properties of QDs are suitable for biological imaging including good photo-stability, strong luminescence, broad excitation spectra and size-tuned fluorescent emission spectra.<sup>68–70</sup> QDs-based nanosensors have been proven to be applicable in cancer diagnosis via cancer-associated proteins and nucleic acid recognition and circulating tumor cell detection.<sup>71–73</sup> However, nanomaterials such as CdS, CdSe and Ag<sub>2</sub>S arouse concern about significant toxicity and environmental hazard due to the risk of leakage of heavy metal elements.<sup>74,75</sup> In this context, outstanding extinction coefficient in near-infrared (NIR) region makes GDY an ideal image agent for cancer. In 2019 Min et al fabricated graphdiyne quantum dots (GDQDs) with uniform size and good crystallization via breakage of graphdiyne oxide nanosheets, which possess excitation- and pH-dependent fluorescence emission.<sup>52</sup> The resistance to photobleaching and high quantum yield facilitate their application. In 2020, Guo et al synthesized a new structure of GDQDs, which linked pyrene groups via Sonogashira cross-coupling reaction.<sup>23</sup> They exhibited superior dispersibility in many organic solvents and water with a high quantum yield of up to 42.8%, revealing their great promise as fluorescent probes.

Photoacoustic imaging (PAI) is now developing into an invasive technique for cancer imaging ascribed to great tissue penetration which provides high spatial resolution within deep tissue. It functions via the photoacoustic effect, converting absorbed light to ultrasonic waves.<sup>76</sup> NIR light-absorbing materials are explored as contrast agents to realize PAI's prospects, which could reduce background interference from PA-active molecules. Various activatable PA probes have been exploited in recent years such as gold nanorods,<sup>77,78</sup> carbon nanostructure<sup>79,80</sup> and organic nanostructures.<sup>81,82</sup> In 2017, Li et al modified graphdiyne nanosheets with PEGylation and evaluated their prospect as a PAI probe in vivo.<sup>83</sup> Under the NIR region, GDY-PEG exhibited a strong photoacoustic signal and distributed uniformly in the tumor site. It displayed competitive photoacoustic stability, the photoacoustic intensity of which was unchanging after 250 laser cycles. This study paved the way for exploring GDY as photoacoustic wave nanotransducer for PAI.

### Therapy

Different from traditional drug delivery, micro/nanocarriers are expected to become powerful active-transport vehicles transporting therapeutic payloads precisely to the desired disease site. Responsive to tumor pathological changes such as pH,<sup>84,85</sup> enzyme expression<sup>86</sup> and temperature,<sup>87,88</sup> nanorobotics transport to target tissue with enhanced therapeutic effect and reduced side effects of drug toxicity. In 2018 Jin et al established doxorubicin (DOX)-loaded GDY nanosheet

which had PH-/photo- dual responsive release behavior for cancer therapy in vitro and in vivo.<sup>89</sup> A highly increased surface area grants GDY with superior DOX loading capacity, which is ascribed to the large  $\pi$ -conjugated architecture. Its DOX-release ability could enhance greatly under laser irradiation. This GDY-based drug delivery platform exhibited promoting cancer inhibition combined with photothermal therapy for high photothermal conversion ability of GDY. In 2020, Yuan et al demonstrated that GDY can release DOX controllably via PH response for HeLa cancer cells inhibition growth, which displayed higher loading (50%) and release DOX capacity (20%) compared with graphene oxide.<sup>90</sup> The rough inner catalytic layer resulting from the nature presence of defects and edges enables GDY to efficiently function at low (0.5%) peroxide levels. In 2021 Xing et al synthesized a multifunctional drug delivery system containing GDYO and three anticancer drugs (DOX, cisplatin (CDDP) and methotrexate (MTX)) and realized photo-chemo synergetic therapy.<sup>91</sup> Due to the high surface area of three-dimensional GDYO-CDDP framework, the nanocarriers exhibited high DOX loading rate of 40.3% with sustained release, which could function as fluorescent trace for drugs as well.

Since the rise of photothermal therapy (PTT), it has aroused great attention in cancer therapy for its appealing merits. Compared to conventional antitumor therapies, PTT has spatiotemporal controllability, high specificity and slight side-effects to normal issues. PTT employs light-absorbing agents to convert optical energy into thermal energy under irradiation of light (like radiofrequency, microwaves and NIR irradiation).<sup>92</sup> The thermal energy efficiently kills tumor cells with minimal nonselective cell death. Outstanding capacity for photothermal conversion under near-infrared irradiation makes GDY an ideal candidate for photothermal therapy. To improve GDY water solubility and biocompatibility, Li et al synthesized GDY with PEGylation in 2017.<sup>83</sup> They demonstrated GDY-PEG's broad absorption band from UV to NIR regions, the mass extinction coefficient of which at 808nm laser irradiation up to  $10.1 \text{ L}\cdot\text{g}^{-1}\cdot\text{cm}^{-1}$ . The photothermal conversion efficiency of GDY-PEG was estimated to be 42%, which was more efficient than classic PTT agents and beneficial for reduction of laser power and irradiation time.<sup>93,94</sup> In 2018, Jin et al employed combined photothermal/chemotherapy with GDY/DOX for cancer treatment.<sup>89</sup> They demonstrated that GDY nanosheet could eliminate cancer cell via hyperthermal effect directly at 808nm laser irradiation, the efficiency of which showed dose dependence. In 2020, Min et al synthesized a tumor-targeting iron sponge (TTIS) nanocomposite based on GDYO, achieving a superior photothermal conversion efficiency of up to 37.5%.<sup>95</sup> The heat produced in the process of PTT promoted Fenton reaction catalyzed by TTIS, thus obtaining combined PTT and enhanced Fenton reaction-mediated cancer therapy.

While cancer is accompanied by intrinsic oxidative stress, reactive oxygen species (ROS), which can cause oxidative damage and induce cellular necrosis and apoptosis, are exploited in cancer cell elimination.<sup>96,97</sup> Chemodynamic therapy (CDT) is an emerging oncotherapy therapy utilizing this redox regulatory mechanisms of cancer cells via Fenton reaction.<sup>98</sup> Responsive to overproduction of hydrogen peroxide in cancer cells,<sup>99</sup> Fenton reaction converses hydrogen peroxide ( $\text{H}_2\text{O}_2$ ) to high-active oxidative hydroxyl radicals (OH) by ferrous ions/ferric ions.<sup>100</sup> The benefits of CDT include high sensitivity and activation by endogenous stimulus. Due to high affinity carbon-carbon triple bonds in graphdiyne oxide for iron, Min et al deposited  $\text{Fe}_3\text{O}_4$  nanoparticles on the surface of GDYO and decorated it with tumor targeting polymer in 2020.<sup>95</sup> With high photothermal conversion efficiency, heat energy produced in the process of PTT enhanced the performance of the Fenton reaction-mediated cancer therapy.

## Radiation Protection

As one of the mainstream cancer treatments in the clinic, radiation therapy can be employed either alone or combined with surgery or chemotherapy.<sup>101–103</sup> It is worth mentioning that the dose of radiation is a double-edged sword, which affects the efficiency of tumor cell killing and imposes damage to adjacent healthy tissue.<sup>104</sup> In this regard, a handful of studies focus on elevating tumor response to radiation and restricting radio-toxicity to normal organs.

Due to  $\pi$ -conjugated system and highly reactive diacetylenic linkages, GDY can absorb electrons and react with free radicals.<sup>105</sup> Such free radical scavenging effects make GDY a promising candidate for application in radioprotection. In 2019, Xie et al synthesized bovine serum albumin-modified GDY nanoparticles (GDY-BSA NPs) and evaluated their free radical scavenging ability (Figure 13).<sup>106</sup> GDY-BSA NPs could not only eliminate free radicals concentration dependently but also clear ROS generated by ionizing radiation to decrease DNA damage in cells and improve their viability. The radioprotection ability of GDY-BSA NPs was further investigated in vivo, which could recover the levels of SOD and MDA exhibiting effective protection to normal tissue.



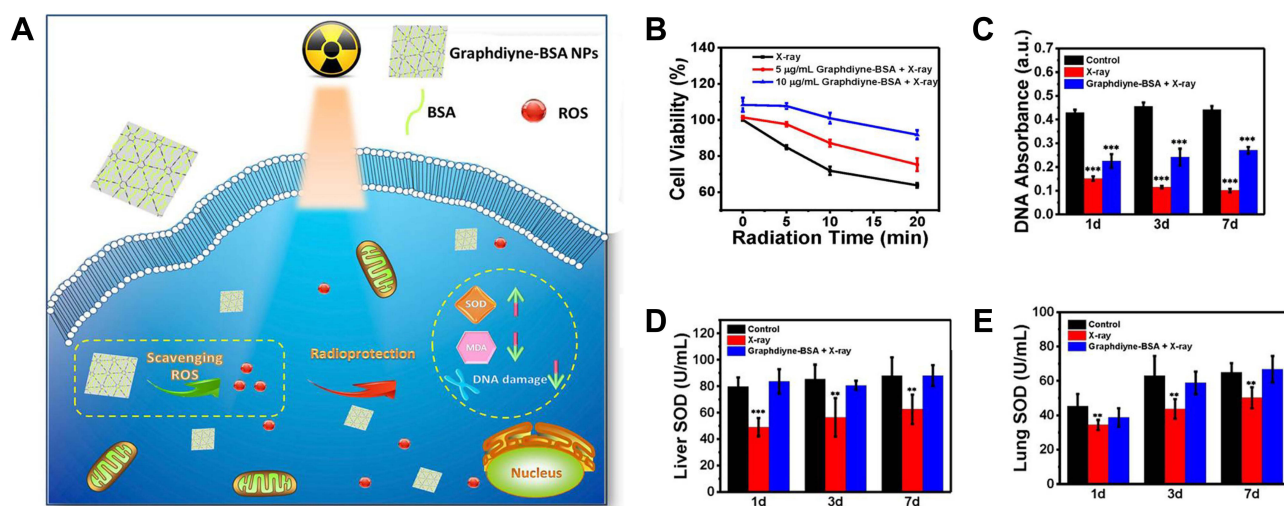


**Figure 13 (A)** Graphdiyne-BSA NPs for radioprotection. **(B)** Radiation dose-dependent protection of HUVECs with or without treatment of graphdiyne-BSA NPs (5 and 10 µg/mL) under different radiation doses. **(C)** DNA damage of mice 1, 3, and 7 days after radiation with or without treatments of graphdiyne-BSA NPs evaluated via UV-vis absorption at 268 nm. **(D and E)** SOD levels in 10% liver and lung homogenate solutions 1, 3, and 7 days after radiation with or without treatment of graphdiyne-BSA NPs.<sup>106</sup>

**Notes:** Reproduced from Xie J, Wang N, Dong X, et al. Graphdiyne nanoparticles with high free radical scavenging activity for radiation protection. *ACS Appl Mater Interfaces*. 2019;11(3):2579–2590. Copyright 2019, American Chemistry Society.<sup>106</sup>

While the control of pelvic and abdominal tumor needs large doses of high energy radiation which induce toxicity to surrounding sensitive gastrointestinal tract and thus cause many gastrointestinal diseases. The team later investigated GDY-BSA NPs as gastrointestinal radioprotectors in 2020 (Figure 14).<sup>107</sup> The excellent chemical stability and relatively long residence time of GDY-BSA NPs in gastric acid environments enabled them to be employed via oral administration, the most convenient way to arrive in the gastrointestinal tract, and fulfill their drug efficacy. In cell models, GDY-BSA NPs relieved DNA of irradiated cells from radiation-induced damage and enhance their viability by inhibiting ROS-induced apoptosis. In animal experiments, these nanoparticles could alleviate irradiation-caused gastrointestinal diseases.

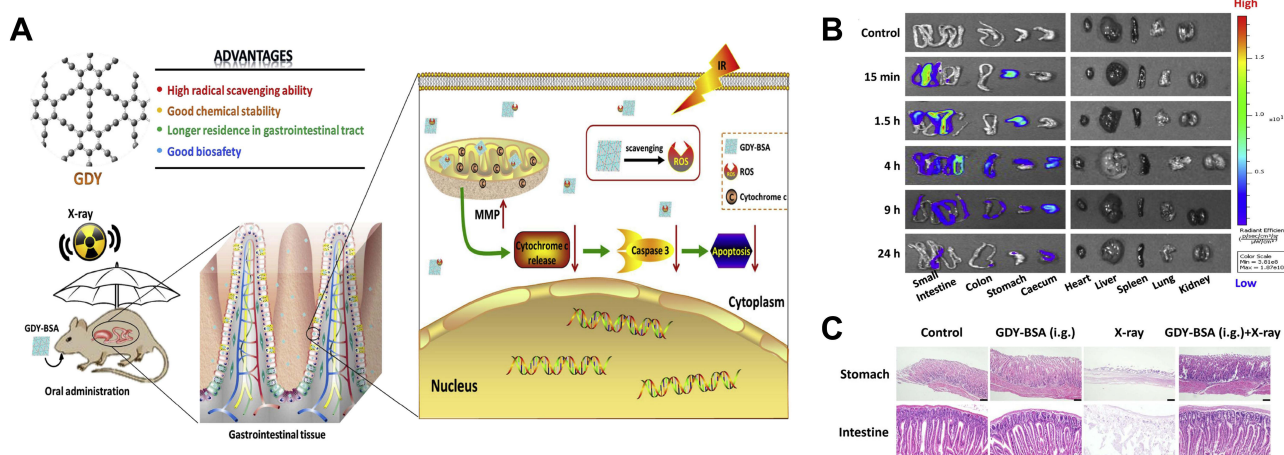


**Figure 14 (A)** Schemes of the GDY-BSA NPs for gastrointestinal radioprotection. **(B)** In vivo fluorescence imaging of various organs in mice after oral administration of GDY-BSA/cyanine NPs at different time points. **(C)** Histopathology analysis of mice after different treatments (including stomach and intestine). Scale bar 50 µm.<sup>107</sup>

**Notes:** Reproduced from Xie J, Wang C, Wang N, et al. Graphdiyne nanoradioprotector with efficient free radical scavenging ability for mitigating radiation-induced gastrointestinal tract damage. *Biomaterials*. 2020;244:119940. Copyright 2020, with permission from Elsevier.<sup>107</sup>

## Tissue Engineering Antibacterial

Anti-infection, especially antibacterial, is a significant issue in tissue engineering improving the therapeutic outcomes. However, traditional antibiotic drugs have encountered the obstacle of antibiotic resistance. Carbon nanomaterials with unique physical and chemical properties are regarded as promising approaches to overcome the limitations of conventional antibiotics and treat drug resistance. They fight pathogenic bacteria efficiently through multiple antibacterial mechanisms simultaneously, including destroying membranes and generating ROS.<sup>108,109</sup>

In 2019, Zhang et al confirmed that GDYO is potent against *Escherichia coli* and *Staphylococcus aureus* dependent on visible light irradiation, bacterial species and time, which sheds light on enhancing the performance of graphdiyne-based nanomaterials (Figure 15).<sup>110</sup> Surface oxidation on GDY nanosheets endowed GDYO better dispersity in an aqueous solution and antibacterial efficiency. Furthermore, the results elucidated three involved antibacterial mechanisms of GDYO: high dispersion in the bacterial suspension, direct contact with bacteria and ROS-dependent oxidation stress. While ROS-dependent oxidation stress is vital, the other two are prerequisites for the ROS mechanism. In 2020, Zhu et al purposed another statement that GDY exhibited better antibacterial ability than GDYO (Figure 16).<sup>111</sup> The broad-spectrum antibacterial behaviors of GYD nanosheets could be ascribed to the synergetic mechanism of wrapping, insertion, disruption and oxidative stress on bacterial membrane and oxidative stress induced by GDY was a minor factor. In 2020, Wang et al synthesized GDY-modified TiO<sub>2</sub> nanofibers to intensify their photocatalytic antibacterial abilities with osteoinductive capacities and improved biocompatibility.<sup>112</sup> TiO<sub>2</sub> has wide application in bone tissue engineering, whereas it may cause infection due to its restrained antibacterial ability resulting from the recombination of generated electrons and holes. Under UV irradiation, GDY with a large surface area and high hole mobility could absorb the free electrons excited from TiO<sub>2</sub>. The reduced recombination rate of electrons and holes in TiO<sub>2</sub> not only improved photocatalytic ROS production for sterilization but also prolonged antibacterial time which could restrict methicillin-resistant *Staphylococcus aureus* biofilm formation at the same time. In 2021, Wang et al utilized GDY as support for palladium (Pd)-iron nanostructure with peroxidase-like activity.<sup>113</sup> This prepared PdFe/GDY exhibited killing bacteria efficiency > 99.99% via depleting glutathione in vitro and was utilized for the treatment of wound infection effectively in vitro. In 2022, Bi et al constructed a boron-doped GDYN for bacteria elimination.<sup>114</sup> It functioned as a peroxidase mimetic nanozyme by decomposing H<sub>2</sub>O<sub>2</sub> to ROS.

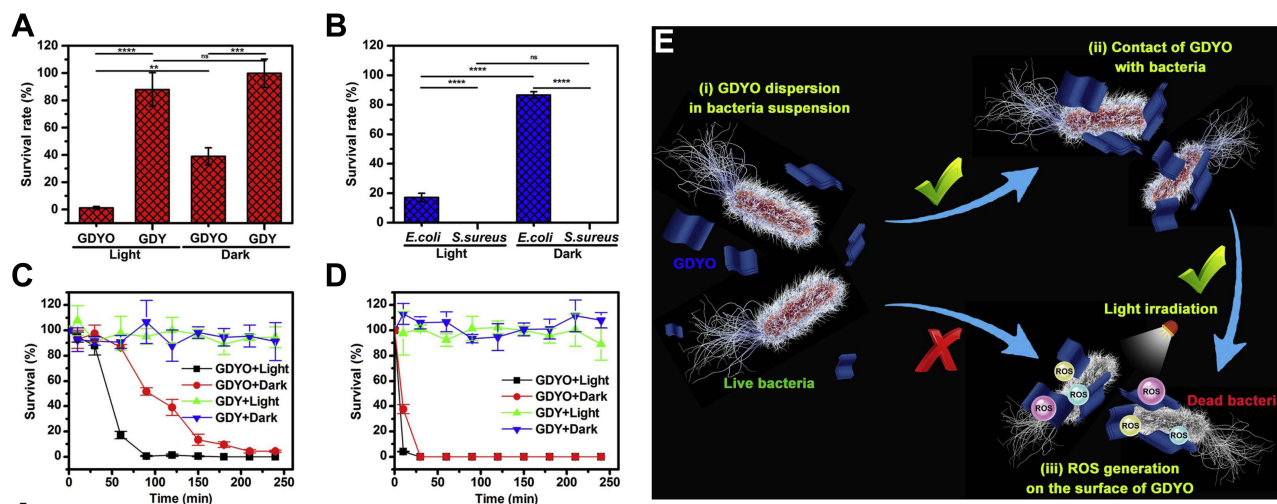


**Figure 15** (A) Survival of *E. coli* after treatment with GDY or GDYO for 120 min in the dark and under visible light irradiation. (B) Survival of *E. coli* and *S. aureus* after treatment with GDYO for 60 min in the dark and under visible light irradiation. Time-dependent antibacterial activity of GDY and GDYO against (C) *E. coli* and (D) *S. aureus* in the dark and under visible light irradiation, respectively. (E) A proposed mechanism for the antibacterial action of a GDYO suspension under visible light irradiation.<sup>110</sup>  
**Notes:** Reproduced from Zhang Y, Liu W, Li Y, Yang YW, Dong A, Li Y. 2D graphdiyne oxide serves as a superior new generation of antibacterial agents. *iScience*. 2019;19:662–675. Copyright 2019, with permission from Elsevier.<sup>110</sup>

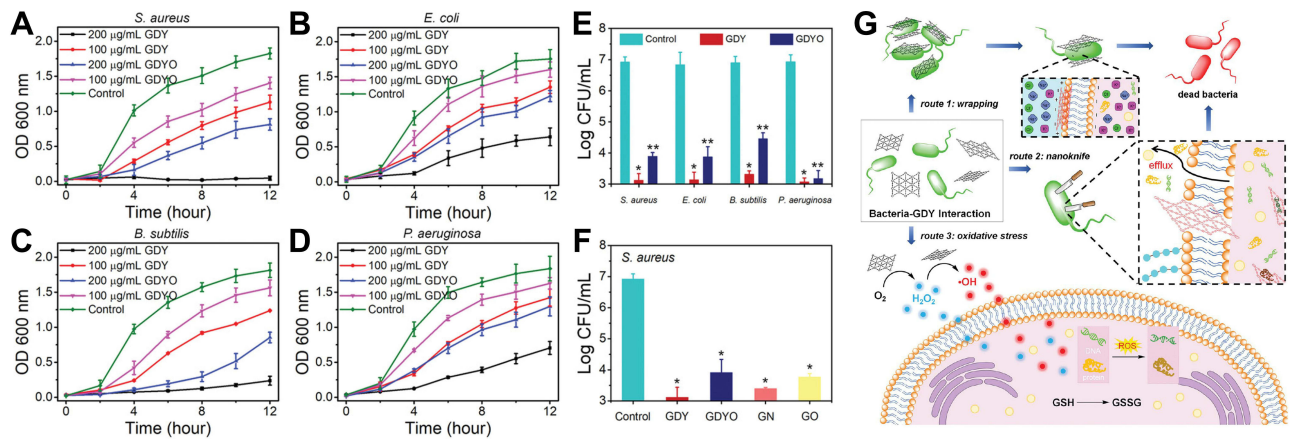


**Figure 16** Growth curves of (A) *S. aureus*, (B) *E. coli*, (C) *B. subtilis*, and (D) *P. aeruginosa* in LB broth fortified with GDY or GDYO. (E) Bacterial cell viability after treatment with GDY or GDYO for 12 h. (F) Comparison of bacterial cell viability after treatment with GDY, GDYO, GN, and GO for 12 h. Ultrapure water was used as control. (G) Illustration of the possible antibacterial mechanisms of GDY-based nanomaterials.<sup>111</sup>

**Notes:** Reproduced from Zhu Z, Bai Q, Li S, et al. Antibacterial activity of graphdiyne and graphdiyne oxide. *Small*. 2020;16(34):2001440. Copyright 2020, John Wiley and Sons.<sup>111</sup>

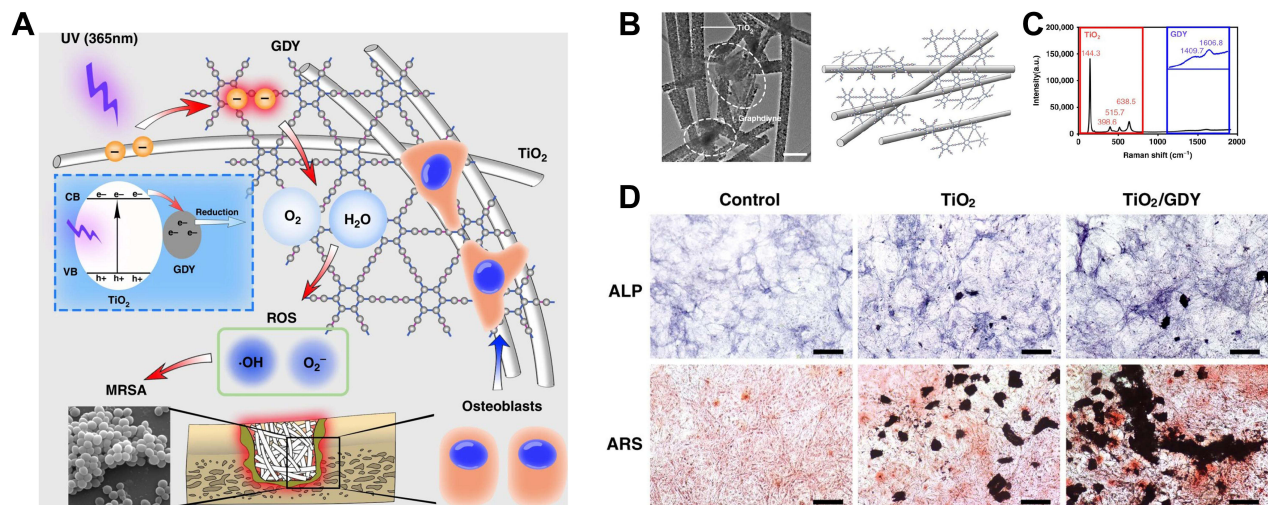


**Figure 17** (A) Schematic of the dual function of  $\text{TiO}_2/\text{GDY}$  in orthopedic implant infection. (B) Transmission electron microscopy of  $\text{TiO}_2/\text{GDY}$  (left, scale bar 0.5  $\mu\text{m}$ , three separate materials) and illustration of the  $\text{TiO}_2/\text{GDY}$  structure (right). (C) Raman spectra of  $\text{TiO}_2/\text{GDY}$ . The main peaks of  $\text{TiO}_2$  are shown in the red box, and the magnified peaks of GDY are shown in blue. (D) Alkaline phosphatase activity and alizarin red S staining for MC3T3-E1 cells treated with  $\text{TiO}_2$ ,  $\text{TiO}_2/\text{GDY}$ , or PBS under osteogenic induction.<sup>112</sup>

**Notes:** Reproduced from Wang R, Shi M, Xu F, et al. Graphdiyne-modified  $\text{TiO}_2$  nanofibers with osteoinductive and enhanced photocatalytic antibacterial activities to prevent implant infection. *Nat Commun*. 2020;11(1):4465. Copyright 2020, The Authors. Creative Commons CCBY License.<sup>112</sup>

## Bone Repair

For the treatment of bone defects, traditional autografts face shortcomings such as hypersensitivity and high incidence of complications.<sup>115–117</sup> In recent years, tissue engineering technology has been seeking artificial substitutes with biological functions. Carbon-based nanomaterials with high biocompatibility, sufficient mechanical properties and large surface area. Increasing studies have demonstrated graphene, the most investigated allotrope of GDY, can induce osteogenic differentiation through several mechanisms, which indicates that GDY possesses osteogenic capability.<sup>118–120</sup> In 2020, Wang et al demonstrated that  $\text{TiO}_2$  modified with GDY improved bone regeneration and sterilization (Figure 17).<sup>112</sup> The GDY nanosheets covered on  $\text{TiO}_2$  strengthened interaction between the compound and biological tissues and osteoinductive abilities for cell adhesion and differentiation.



## Conclusion

Since the first synthesis in 2010, GDY has attracted increasing attention and studies towards this planar layered-materials. Highly conjugated  $\pi$  bonding, uniformly distributed pores and linear acetylenic linkages endow GDY with great prospects in wide application. Fabricating this novel carbon allotrope with different morphologies is a reliable approach to enhancing its electronic and mechanical properties. In this review, we have summarized current advances in structure-controlled synthesis for GDY. Different morphologies of GDY like quantum dots, nanotubes, nanowires, nanoribbons, nanowalls, nanosheets, ordered stripe arrays and nanospheres have prompted its development, turning the theoretical prediction of GDY into possible applications. Extraordinary efforts have been paid to realize GDY's practical use in the field of photocatalysis, electrocatalysis, energy storage, etc., which exhibits greater potential than many other carbon materials. This review outlines the promising biomedical applications of GDY and its derivatives. Owing to the carbon triple bonds, GDY has a high capacity for atoms and in situ catalysis, which facilitates it to become sensitive and selective biosensors for some molecules in human. Optical properties and loading capacity make GDY a versatile theranostic platform for cancer. GDY displays resistance to radiation and bacteria.

However, studies of GDY are still in their infancy and moving GDY and its derivatives from experimental studies to the clinical practice still requires much efforts. First, because the limited yield of GDY restricts its practical applications, large-scale and cost-effective production should be the theme of future research. Meanwhile, manufacturing of GDY-based materials with reproducibility and reliability is necessary as batch-to-batch variations would affect their physicochemical properties. Secondly, massive clinical trials and studies are needed to investigate the behavior and functionality of GDY-based materials before their practical uses, such as metabolism, biocompatibility, biodegradability and toxicity. Despite studies indicating that GDY and its derivatives are safer than other carbon-based materials, the biotoxicity of GDY remains unknown, which is highly affected by their particular form, such as the size, morphology, chemical structure. Thus, a thoroughgoing understanding of short-term and long-term toxicity profile of GDY in vitro and in vivo is required. Third, efforts should be taken in precisely and accurately constructing nanostructured GDY with designed size and morphologies or modifying GDY via chemical functionalization and doping. This could endow GDY with improved physical, chemical and electrical properties and develop applications of GDY and its derivatives in various fields.

In summary, GDY-based nanomaterials with unique advantages are promising in biomedical applications, yet there are problems remaining to be addressed to bring GDY from theoretical research to the clinic. We believe that these challenges will be resolved and GDY will play a more significant role in biomedical applications.

## Acknowledgment

This work was supported by grants from the fellowship of the Guangzhou Science and Technology Plan Project (202201011527) and Guangdong Basic and Applied Basic Research Foundation (2021A1515110267).

## Disclosure

The authors report no conflicts of interest in this work.

## References

1. Kroto HW, Heath JR, O'Brien SC, Curl RF, Smalley RE. C 60: buckminsterfullerene. *Nature*. 1985;318(6042):162–163. doi:10.1038/318162a0
2. Iijima S. Helical microtubules of graphitic carbon. *Nature*. 1991;354(6348):56–58. doi:10.1038/354056a0
3. Novoselov KS, Geim AK, Morozov SV. Electric field effect in atomically thin carbon films. *Science*. 2004;306(5696):666–669. doi:10.1126/science.1102896
4. Baughman RH, Eckhardt H, Kertesz M. Structure-property predictions for new planar forms of carbon: layered phases containing  $sp^2$  and  $sp$  atoms. *J Chem Phys*. 1987;87(11):6687–6699. doi:10.1063/1.453405
5. Wan WB, Haley MM. Carbon networks based on dehydrobenzoannulenes. 4. Synthesis of “star” and “trefoil” graphdiyne substructures via sixfold cross-coupling of hexaiodobenzene. *J Org Chem*. 2001;66(11):3893–3901. doi:10.1021/jo010183n
6. Marsden JA, Haley MM. Carbon networks based on dehydrobenzoannulenes. 5. Extension of two-dimensional conjugation in graphdiyne nanoarchitectures. *J Org Chem*. 2005;70(25):10213–10226. doi:10.1021/jo050926v
7. Li G, Li Y, Liu H, Guo Y, Li Y, Zhu D. Architecture of graphdiyne nanoscale films. *Chem Commun*. 2010;46(19):3256–3258. doi:10.1039/b922733d
8. Wan WB, Brand SC, Pak JJ, Haley MM. Synthesis of expanded graphdiyne substructures. *Chem Weinh Bergstr Ger*. 2000;6(11):2044–2052. doi:10.1002/1521-3765(20000602)6:11<2044::aid-chem2044>3.0.co;2-y



9. Tan J, He X, Zhao M. First-principles study of hydrogenated graphyne and its family: stable configurations and electronic structures. *Diam Relat Mater.* 2012;29:42–47. doi:10.1016/j.diamond.2012.07.006
10. Pan Q, Liu H, Zhao Y, et al. Preparation of N-graphdiyne nanosheets at liquid/liquid interface for photocatalytic NADH regeneration. *ACS Appl Mater Interfaces.* 2019;11(3):2740–2744. doi:10.1021/acsami.8b03311
11. Li Y, Fang Y, Xue Y, Hui L, Yu H. Graphdiyne@Janus magnetite for photocatalysis nitrogen fixation. *Angew Chem Int Ed.* 2020. doi:10.1002/anie.202012357
12. Su K, Dong GX, Zhang W, Liu ZL, Zhang M, Lu TB. In situ coating CsPbBr<sub>3</sub> nanocrystals with graphdiyne to boost the activity and stability of photocatalytic CO<sub>2</sub> reduction. *ACS Appl Mater Interfaces.* 2020;12(45):50464–50471. doi:10.1021/acsami.0c14826
13. Yin XP, Wang HJ, Tang SF, et al. Engineering the coordination environment of single-atom platinum anchored on graphdiyne for optimizing electrocatalytic hydrogen evolution. *Angew Chem Int Ed.* 2018;57(30):9382–9386. doi:10.1002/anie.201804817
14. Xue Y, Huang B, Yi Y, et al. Anchoring zero valence single atoms of nickel and iron on graphdiyne for hydrogen evolution. *Nat Commun.* 2018;9(1):1460. doi:10.1038/s41467-018-03896-4
15. Wang N, He J, Tu Z, et al. Synthesis of chlorine-substituted graphdiyne and applications for lithium-ion storage. *Angew Chem Int Ed.* 2017;56(36):10740–10745. doi:10.1002/anie.201704779
16. Wang K, Wang N, He J, Yang Z, Shen X, Huang C. Preparation of 3D architecture graphdiyne nanosheets for high-performance sodium-ion batteries and capacitors. *ACS Appl Mater Interfaces.* 2017;9(46):40604–40613. doi:10.1021/acsami.7b11420
17. Shang H, Zuo Z, Li L, et al. Ultrathin graphdiyne nanosheets grown in situ on copper nanowires and their performance as lithium-ion battery anodes. *Angew Chem Int Ed.* 2018;57(3):774–778. doi:10.1002/anie.201711366
18. Lv JX, Zhang ZM, Wang J, Lu XL, Zhang W, Lu TB. In situ synthesis of CdS/graphdiyne heterojunction for enhanced photocatalytic activity of hydrogen production. *ACS Appl Mater Interfaces.* 2019;11(3):2655–2661. doi:10.1021/acsami.8b03326
19. Gao X, Zhou J, Du R, et al. Robust superhydrophobic foam: a graphdiyne-based hierarchical architecture for oil/water separation. *Adv Mater.* 2016;28(1):168–173. doi:10.1002/adma.201504407
20. Yan H, Guo S, Wu F, et al. Carbon atom hybridization matters: ultrafast humidity response of graphdiyne oxides. *Angew Chem Int Ed.* 2018;57(15):3922–3926. doi:10.1002/anie.201709417
21. Zheng T, Gao Y, Deng X, et al. Comparisons between graphene oxide and graphdiyne oxide in physicochemistry biology and cytotoxicity. *ACS Appl Mater Interfaces.* 2018;10(39):32946–32954. doi:10.1021/acsami.8b06804
22. Abbasi E, Kafshdooz T, Bakhtiari M, et al. Biomedical and biological applications of quantum dots. *Artif Cells Nanomed Biotechnol.* 2015:1–7. doi:10.3109/21691401.2014.998826
23. Guo J, Guo M, Wang F, et al. Graphdiyne: structure of fluorescent quantum dots. *Angew Chem Int Ed.* 2020;59(38):16712–16716. doi:10.1002/anie.202006891
24. Li G, Li Y, Qian X, et al. Construction of tubular molecule aggregations of graphdiyne for highly efficient field emission. *J Phys Chem C.* 2011;115(6):2611–2615. doi:10.1021/jp107996f
25. Jalili S, Houshmand F, Schofield J. Study of carrier mobility of tubular and planar graphdiyne. *Appl Phys A.* 2015;119(2):571–579. doi:10.1007/s00339-015-8992-8
26. Shohany BG, Roknabadi MR, Kompany A. Computational study of edge configuration and the diameter effects on the electrical transport of graphdiyne nanotubes. *Phys E Low Dimens Syst Nanostructures.* 2016;84:146–151. doi:10.1016/j.physe.2016.05.040
27. Pari S, Cuéllar A, Wong BM. Structural and electronic properties of graphdiyne carbon nanotubes from large-scale DFT calculations. *J Phys Chem C.* 2016;120(33):18871–18877. doi:10.1021/acs.jpcc.6b05265
28. Qian X, Ning Z, Li Y, et al. Construction of graphdiyne nanowires with high-conductivity and mobility. *Dalton Trans.* 2012;41(3):730–733. doi:10.1039/C1DT11641J
29. Cirera B, Zhang YQ, Björk J, et al. Synthesis of extended graphdiyne wires by vicinal surface templating. *Nano Lett.* 2014;14(4):1891–1897. doi:10.1021/nl4046747
30. Klappenberger F, Hellwig R, Du P, et al. Functionalized graphdiyne nanowires: on-surface synthesis and assessment of band structure, flexibility, and information storage potential. *Small.* 2018;14(14):1704321. doi:10.1002/sml.201704321
31. Zhou W, Shen H, Zeng Y, et al. Controllable synthesis of graphdiyne nanoribbons. *Angew Chem Int Ed.* 2020;59(12):4908–4913. doi:10.1002/anie.201916518
32. Long M, Tang L, Wang D, Li Y, Shuai Z. Electronic structure and carrier mobility in graphdiyne sheet and nanoribbons: theoretical predictions. *ACS Nano.* 2011;5(4):2593–2600. doi:10.1021/nn102472s
33. Pan LD, Zhang LZ, Song BQ, Du SX, Gao HJ. Graphyne- and graphdiyne-based nanoribbons: density functional theory calculations of electronic structures. *Appl Phys Lett.* 2011;98(17):173102. doi:10.1063/1.3583507
34. Zhou J, Gao X, Liu R, et al. Synthesis of graphdiyne nanowalls using acetylenic coupling reaction. *J Am Chem Soc.* 2015;137(24):7596–7599.
35. Gao X, Li J, Du R, et al. Direct synthesis of graphdiyne nanowalls on arbitrary substrates and its application for photoelectrochemical water splitting cell. *Adv Mater.* 2017;29(9):1605308. doi:10.1002/adma.201605308
36. Zhang S, Yin C, Kang Z, et al. Graphdiyne nanowall for enhanced photoelectrochemical performance of Si heterojunction photoanode. *ACS Appl Mater Interfaces.* 2019;11(3):2745–2749. doi:10.1021/acsami.8b06382
37. Matsuoka R, Sakamoto R, Hoshiko K, et al. Crystalline graphdiyne nanosheets produced at a gas/liquid or liquid/liquid interface. *J Am Chem Soc.* 2017;139(8):3145–3152. doi:10.1021/jacs.6b12776
38. Shang H, Zuo Z, Zheng H, et al. N-doped graphdiyne for high-performance electrochemical electrodes. *Nano Energy.* 2018;44:144–154. doi:10.1016/j.nanoen.2017.11.072
39. Navae A, Salimi A, Sham TK. Bipolar electrochemistry as a powerful technique for rapid synthesis of ultrathin graphdiyne nanosheets: improvement of photoelectrocatalytic activity toward both hydrogen and oxygen evolution. *Int J Hydrog Energy.* 2021;46(24):12906–12914. doi:10.1016/j.ijhydene.2021.01.117
40. Wang SS, Liu HB, Kan XN, et al. Superlyophilicity-facilitated synthesis reaction at the microscale: ordered graphdiyne stripe arrays. *Small.* 2017;13(4):1602265. doi:10.1002/sml.201602265
41. Yu J, Chen W, Li K, et al. Graphdiyne nanospheres as a wettability and electron modifier for enhanced hydrogenation catalysis. *Angew Chem Int Ed.* 2022;61(34):e202207255. doi:10.1002/anie.202207255

42. Zhu C, Zeng Z, Li H, Li F, Fan C, Zhang H. Single-layer MoS<sub>2</sub>-based nanoprobe for homogeneous detection of biomolecules. *J Am Chem Soc.* 2013;135(16):5998–6001. doi:10.1021/ja401957z
43. Wang Q, Wang W, Lei J, Xu N, Gao F, Ju H. Fluorescence quenching of carbon nitride nanosheet through its interaction with DNA for versatile fluorescence sensing. *Anal Chem.* 2013;85(24):12182–12188. doi:10.1021/ac403646n
44. Peng H, Zhang L, Kjällman THM, Soeller C. DNA hybridization detection with blue luminescent quantum dots and dye-labeled single-stranded DNA. *J Am Chem Soc.* 2007;129(11):3048–3049. doi:10.1021/ja0685452
45. Wang C, Yu P, Guo S, Mao L, Liu H, Li Y. Graphdiyne oxide as a platform for fluorescence sensing. *Chem Commun.* 2016;52(32):5629–5632. doi:10.1039/C6CC01856D
46. Parvin N, Jin Q, Wei Y, et al. Few-layer graphdiyne nanosheets applied for multiplexed real-time DNA detection. *Adv Mater.* 2017;29(18):1606755. doi:10.1002/adma.201606755
47. Chang F, Huang L, Guo C, Xie G, Li J, Diao Q. Graphdiyne-based one-step DNA fluorescent sensing platform for the detection of *Mycobacterium tuberculosis* and its drug-resistant genes. *ACS Appl Mater Interfaces.* 2019;11(39):35622–35629. doi:10.1021/acsami.9b15248
48. Barham D, Trinder P. An improved colour reagent for the determination of blood glucose by the oxidase system. *Analyst.* 1972;97(1151):142. doi:10.1039/an9729700142
49. Liu J, Shen X, Baimanov D, et al. Immobilized ferrous ion and glucose oxidase on graphdiyne and its application on one-step glucose detection. *ACS Appl Mater Interfaces.* 2019;11(3):2647–2654. doi:10.1021/acsami.8b03118
50. Zhu Q, Yuan Y, Yan B, Zhou J, Zuo J, Bai L. A new biomimetic nanozyme of hemin/graphdiyne oxide with superior peroxidase-like activity for colorimetric bioassays. *Analyst.* 2021;146(23):7284–7293. doi:10.1039/D1AN01456K
51. Chen X, Gao P, Guo L, Zhang S. Graphdiyne as a promising material for detecting amino acids. *Sci Rep.* 2015;5(1):16720. doi:10.1038/srep16720
52. Min H, Qi Y, Chen Y, et al. Synthesis and imaging of biocompatible graphdiyne quantum dots. *ACS Appl Mater Interfaces.* 2019;11(36):32798–32807. doi:10.1021/acsami.9b12801
53. Bai Q, Zhang C, Li L, et al. Subsequent monitoring of ferric ion and ascorbic acid using graphdiyne quantum dots-based optical sensors. *Microchim Acta.* 2020;187(12):657. doi:10.1007/s00604-020-04624-w
54. Hu Z, Yang W, Liu H, et al. From PET/CT to PET/MRI: advances in instrumentation and clinical applications. *Mol Pharm.* 2014;11(11):3798–3809. doi:10.1021/mp500321h
55. Hasebroock KM, Serkova NJ. Toxicity of MRI and CT contrast agents. *Expert Opin Drug Metab Toxicol.* 2009;5(4):403–416. doi:10.1517/17425250902873796
56. Yang L, Yin X, Gai P, Li F. A label-free homogeneous electrochemical cytosensor for the ultrasensitive detection of cancer cells based on multiaptamer-functionalized DNA tetrahedral nanostructures. *Chem Commun.* 2020;56(27):3883–3886. doi:10.1039/D0CC00788A
57. Sun Y, Yuan B, Deng M, et al. A light-up fluorescence assay for tumor cell detection based on bifunctional split aptamers. *Analyst.* 2018;143(15):3579–3585. doi:10.1039/C8AN01008K
58. Li H, Lin H, Lv W, Gai P, Li F. Equipment-free and visual detection of multiple biomarkers via an aggregation induced emission luminogen-based paper biosensor. *Biosens Bioelectron.* 2020;165:112336. doi:10.1016/j.bios.2020.112336
59. Zhao WW, Xu JJ, Chen HY. Photoelectrochemical DNA biosensors. *Chem Rev.* 2014;114(15):7421–7441. doi:10.1021/cr500100j
60. Li M, Meng G, Huang Q, Zhang S. Improved sensitivity of polychlorinated-biphenyl-orientated porous-ZnO surface photovoltage sensors from chemisorption-formed ZnO-CuPc composites. *Sci Rep.* 2015;4(1):4284. doi:10.1038/srep04284
61. Cui L, Shen J, Li CC, et al. Construction of a dye-sensitized and gold plasmon-enhanced cathodic photoelectrochemical biosensor for methyltransferase activity assay. *Anal Chem.* 2021;93(29):10310–10316. doi:10.1021/acs.analchem.1c01797
62. Fan GC, Zhu H, Shen Q, et al. Enhanced photoelectrochemical aptasensing platform based on exciton energy transfer between CdSeTe alloyed quantum dots and SiO<sub>2</sub>@Au nanocomposites. *Chem Commun.* 2015;51(32):7023–7026. doi:10.1039/c5cc01935d
63. Tseng KW, Hsiao YP, Jen CP, Chang TS, Wang HC. Cu<sub>2</sub>O/PEDOT:PSS/ZnO nanocomposite material biosensor for esophageal cancer detection. *Sensors.* 2020;20(9):E2455. doi:10.3390/s20092455
64. Li J, Gao X, Liu B, et al. Graphdiyne: a metal-free material as hole transfer layer to fabricate quantum dot-sensitized photocathodes for hydrogen production. *J Am Chem Soc.* 2016;138(12):3954–3957. doi:10.1021/jacs.5b12758
65. Li Y, Li X, Meng Y, Hun X. Photoelectrochemical platform for MicroRNA let-7a detection based on graphdiyne loaded with AuNPs modified electrode coupled with alkaline phosphatase. *Biosens Bioelectron.* 2019;130:269–275. doi:10.1016/j.bios.2019.02.002
66. Lu J, Getz G, Miska EA, et al. MicroRNA expression profiles classify human cancers. *Nature.* 2005;435(7043):834–838. doi:10.1038/nature03702
67. Medintz IL, Uyeda HT, Goldman ER, Mattoussi H. Quantum dot bioconjugates for imaging, labelling and sensing. *Nat Mater.* 2005;4(6):435–446. doi:10.1038/nmat1390
68. Bruchez M, Moronne M, Gin P, Weiss S, Alivisatos AP. Semiconductor nanocrystals as fluorescent biological labels. *Science.* 1998;281(5385):2013–2016. doi:10.1126/science.281.5385.2013
69. Chan WC, Nie S. Quantum dot bioconjugates for ultrasensitive nonisotopic detection. *Science.* 1998;281(5385):2016–2018. doi:10.1126/science.281.5385.2016
70. Qu L, Peng X. Control of photoluminescence properties of CdSe nanocrystals in growth. *J Am Chem Soc.* 2002;124(9):2049–2055. doi:10.1021/ja017002j
71. Han M, Gao X, Su JZ, Nie S. Quantum-dot-tagged microbeads for multiplexed optical coding of biomolecules. *Nat Biotechnol.* 2001;19(7):631–635. doi:10.1038/90228
72. Tian J, Zhou L, Zhao Y, Wang Y, Peng Y, Zhao S. Multiplexed detection of tumor markers with multicolor quantum dots based on fluorescence polarization immunoassay. *Talanta.* 2012;92:72–77. doi:10.1016/j.talanta.2012.01.051
73. Wen CY, Wu LL, Zhang ZL, et al. Quick-response magnetic nanospheres for rapid, efficient capture and sensitive detection of circulating tumor cells. *ACS Nano.* 2014;8(1):941–949. doi:10.1021/nn405744f
74. Winnik FM, Maysinger D. Quantum dot cytotoxicity and ways to reduce it. *Acc Chem Res.* 2013;46(3):672–680. doi:10.1021/ar3000585
75. Kumar A, Kumar P. Cytotoxicity of quantum dots: use of quasiSMILES in development of reliable models with index of ideality of correlation and the consensus modelling. *J Hazard Mater.* 2021;402:123777. doi:10.1016/j.jhazmat.2020.123777

76. Wang LV, Hu S. Photoacoustic tomography: in vivo imaging from organelles to organs. *Science*. 2012;335(6075):1458–1462. doi:10.1126/science.1216210
77. Manivasagan P, Bharathiraja S, Santha Moorthy M, et al. Anti-EGFR antibody conjugation of fucoidan-coated gold nanorods as novel photothermal ablation agents for cancer therapy. *ACS Appl Mater Interfaces*. 2017;9(17):14633–14646. doi:10.1021/acsami.7b00294
78. Cheng K, Kothapalli SR, Liu H, et al. Construction and validation of nano gold tripods for molecular imaging of living subjects. *J Am Chem Soc*. 2014;136(9):3560–3571. doi:10.1021/ja412001e
79. Wang C, Bao C, Liang S, et al. RGD-conjugated silica-coated gold nanorods on the surface of carbon nanotubes for targeted photoacoustic imaging of gastric cancer. *Nanoscale Res Lett*. 2014;9(1):264. doi:10.1186/1556-276X-9-264
80. de la Zerda A, Liu Z, Bodapati S, et al. Ultrahigh sensitivity carbon nanotube agents for photoacoustic molecular imaging in living mice. *Nano Lett*. 2010;10(6):2168–2172. doi:10.1021/nl100890d
81. Pu K, Shuhendler AJ, Jakerst JV, et al. Semiconducting polymer nanoparticles as photoacoustic molecular imaging probes in living mice. *Nat Nanotechnol*. 2014;9(3):233–239. doi:10.1038/nnano.2013.302
82. Lovell JF, Jin CS, Huynh E, et al. Porphyrin bilayers generated by porphyrin bilayers for use as multimodal biophotonic contrast agents. *Nat Mater*. 2011;10(4):324–332. doi:10.1038/nmat2986
83. Li S, Chen Y, Liu H, et al. Graphdiyne materials as nanotransducer for in vivo photoacoustic imaging and photothermal therapy of tumor. *Chem Mater*. 2017;29(14):6087–6094. doi:10.1021/acs.chemmater.7b01965
84. Jelezova I, Drakalska E, Momekova D, et al. Curcumin loaded pH-sensitive hybrid lipid/block copolymer nanosized drug delivery systems. *Eur J Pharm Sci*. 2015;78:67–78. doi:10.1016/j.ejps.2015.07.005
85. de Barros ALB, Mota LD, Soares DC, et al. Long-circulating, pH-sensitive liposomes versus long-circulating, non-pH-sensitive liposomes as a delivery system for tumor identification. *J Biomed Nanotechnol*. 2013;9(9):1636–1643. doi:10.1166/jbn.2013.1649
86. Kawano T, Tachibana Y, Inokuchi J, Kang JH, Murata M, Eto M. Identification of activated protein kinase Ca (PKCa) in the urine of orthotopic bladder cancer xenograft model as a potential biomarker for the diagnosis of bladder cancer. *Int J Mol Sci*. 2021;22(17):9276. doi:10.3390/ijms22179276
87. Lee JH, Tachibana T, Yamana K, Kawasaki R, Yabuki A. Simple formation of cancer drug-containing self-assembled hydrogels with temperature and pH-responsive release. *Langmuir*. 2021;37(38):11269–11275. doi:10.1021/acs.langmuir.1c01700
88. Farjadian F, Rezaeifard S, Naeimi M, et al. Temperature and pH-responsive nano-hydrogel drug delivery system based on lysine-modified poly (vinylcaprolactam). *Int J Nanomedicine*. 2019;14:6901–6915. doi:10.2147/IJN.S214467
89. Jin J, Guo M, Liu J, et al. Graphdiyne nanosheet-based drug delivery platform for photothermal/chemotherapy combination treatment of cancer. *ACS Appl Mater Interfaces*. 2018;10(10):8436–8442. doi:10.1021/acsami.7b17219
90. Yuan K, Asunción-Nadal V, Li Y, Jurado-Sánchez B, Escarpa A. Graphdiyne micromotors in living biomed. *Chem Eur J*. 2020;26(38):8471–8477. doi:10.1002/chem.202001754
91. Xue Z, Zhu M, Dong Y, et al. An integrated targeting drug delivery system based on the hybridization of graphdiyne and MOFs for visualized cancer therapy. *Nanoscale*. 2019;11(24):11709–11718. doi:10.1039/C9NR02017A
92. Jaque D, Martínez Maestro L, Del Rosal B, et al. Nanoparticles for photothermal therapies. *Nanoscale*. 2014;6(16):9494–9530. doi:10.1039/c4nr00708e
93. Tian Q, Jiang F, Zou R, et al. Hydrophilic Cu9S5 nanocrystals: a photothermal agent with a 25.7% heat conversion efficiency for photothermal ablation of cancer cells in vivo. *ACS Nano*. 2011;5(12):9761–9771. doi:10.1021/nn203293t
94. Hessel CM, Pattani VP, Rasch M, et al. Copper selenide nanocrystals for photothermal therapy. *Nano Lett*. 2011;11(6):2560–2566. doi:10.1021/nl201400z
95. Min H, Qi Y, Zhang Y, et al. A graphdiyne oxide-based iron sponge with photothermally enhanced tumor-specific Fenton chemistry. *Adv Mater*. 2020;32(31):2000038. doi:10.1002/adma.202000038
96. López-Lázaro M. Dual role of hydrogen peroxide in cancer: possible relevance to cancer chemoprevention and therapy. *Cancer Lett*. 2007;252(1):1–8. doi:10.1016/j.canlet.2006.10.029
97. Trachootham D, Alexandre J, Huang P. Targeting cancer cells by ROS-mediated mechanisms: a radical therapeutic approach? *Nat Rev Drug Discov*. 2009;8(7):579–591. doi:10.1038/nrd2803
98. Tang Z, Liu Y, He M, Bu W. Chemodynamic therapy: tumour microenvironment-mediated Fenton and Fenton-like reactions. *Angew Chem Int Ed*. 2019;58(4):946–956. doi:10.1002/anie.201805664
99. Chen Q, Liang C, Sun X, et al. H2O2-responsive liposomal nanoprobe for photoacoustic inflammation imaging and tumor theranostics via in vivo chromogenic assay. *Proc Natl Acad Sci U S A*. 2017;114(21):5343–5348. doi:10.1073/pnas.1701976114
100. Zhang C, Bu W, Ni D, et al. Synthesis of iron nanometallic glasses and their application in cancer therapy by a localized Fenton reaction. *Angew Chem Int Ed*. 2016;55(6):2101–2106. doi:10.1002/anie.201510031
101. Trovo M, Furlan C, Polesel J, et al. Radical radiation therapy for oligometastatic breast cancer: results of a prospective Phase II trial. *Radiother Oncol*. 2018;126(1):177–180. doi:10.1016/j.radonc.2017.08.032
102. Ngan SY, Burmeister B, Fisher RJ, et al. Randomized trial of short-course radiotherapy versus long-course chemoradiation comparing rates of local recurrence in patients with T3 rectal cancer: trans-Tasman radiation oncology group trial 01.04. *J Clin Oncol*. 2012;30(31):3827–3833. doi:10.1200/JCO.2012.42.9597
103. Hamilton SN, Tyldesley S, Li D, Olson R, McBride M. Second malignancies after adjuvant radiation therapy for early stage breast cancer: is there increased risk with addition of regional radiation to local radiation? *Int J Radiat Oncol*. 2015;91(5):977–985. doi:10.1016/j.ijrobp.2014.12.051
104. Rannou E, François A, Toullec A, et al. In vivo evidence for an endothelium-dependent mechanism in radiation-induced normal tissue injury. *Sci Rep*. 2015;5(1):15738. doi:10.1038/srep15738
105. Grebowksi J, Krokosz A, Konarska A, Wolszczak M, Puchala M. Rate constants of highly hydroxylated fullerene C60 interacting with hydroxyl radicals and hydrated electrons. Pulse radiolysis study. *Radiat Phys Chem*. 2014;103:146–152. doi:10.1016/j.radphyschem.2014.05.057
106. Xie J, Wang N, Dong X, et al. Graphdiyne nanoparticles with high free radical scavenging activity for radiation protection. *ACS Appl Mater Interfaces*. 2019;11(3):2579–2590. doi:10.1021/acsami.8b00949

107. Xie J, Wang C, Wang N, et al. Graphdiyne nanoradioprotector with efficient free radical scavenging ability for mitigating radiation-induced gastrointestinal tract damage. *Biomaterials*. 2020;244:119940. doi:10.1016/j.biomaterials.2020.119940
108. Li H, Huang J, Song Y, et al. Degradable carbon dots with broad-spectrum antibacterial activity. *ACS Appl Mater Interfaces*. 2018;10(32):26936–26946. doi:10.1021/acsami.8b08832
109. Zhong L, Liu H, Samal M, Yun K. Synthesis of ZnO nanoparticles-decorated spindle-shaped graphene oxide for application in synergistic antibacterial activity. *J Photochem Photobiol B*. 2018;183:293–301. doi:10.1016/j.jphotobiol.2018.04.048
110. Zhang Y, Liu W, Li Y, Yang YW, Dong A, Li Y. 2D graphdiyne oxide serves as a superior new generation of antibacterial agents. *iScience*. 2019;19:662–675. doi:10.1016/j.isci.2019.08.019
111. Zhu Z, Bai Q, Li S, et al. Antibacterial activity of graphdiyne and graphdiyne oxide. *Small*. 2020;16(34):2001440. doi:10.1002/sml.202001440
112. Wang R, Shi M, Xu F, et al. Graphdiyne-modified TiO<sub>2</sub> nanofibers with osteoinductive and enhanced photocatalytic antibacterial activities to prevent implant infection. *Nat Commun*. 2020;11(1):4465. doi:10.1038/s41467-020-18267-1
113. Wang T, Bai Q, Zhu Z, et al. Graphdiyne-supported palladium-iron nanosheets: a dual-functional peroxidase mimetic nanozyme for glutathione detection and antibacterial application. *Chem Eng J*. 2021;413:127537. doi:10.1016/j.cej.2020.127537
114. Bi X, Bai Q, Wang L, et al. Boron doped graphdiyne: a metal-free peroxidase mimetic nanozyme for antibacterial application. *Nano Res*. 2022;15(2):1446–1454. doi:10.1007/s12274-021-3685-4
115. Nayak TR, Jian L, Phua LC, Ho HK, Ren Y, Pastorin G. Thin films of functionalized multiwalled carbon nanotubes as suitable scaffold materials for stem cells proliferation and bone formation. *ACS Nano*. 2010;4(12):7717–7725. doi:10.1021/nn102738c
116. Liao CZ, Li K, Wong HM, Tong WY, Yeung KWK, Tjong SC. Novel polypropylene biocomposites reinforced with carbon nanotubes and hydroxyapatite nanorods for bone replacements. *Mater Sci Eng C Mater Biol Appl*. 2013;33(3):1380–1388. doi:10.1016/j.msec.2012.12.039
117. Li JL, Yang Z, Loo WT, et al. In vitro and in vivo biocompatibility of multi-walled carbon nanotube/biodegradable polymer nanocomposite for bone defects repair. *J Bioact Compat Polym*. 2014;29(4):350–367. doi:10.1177/0883911514533867
118. Elkhenany H, Amelse L, Lafont A, et al. Graphene supports in vitro proliferation and osteogenic differentiation of goat adult mesenchymal stem cells: potential for bone tissue engineering. *J Appl Toxicol*. 2015;35(4):367–374. doi:10.1002/jat.3024
119. Dubey N, Morin JLP, Luong-Van EK, et al. Osteogenic potential of graphene coated titanium is independent of transfer technique. *Materialia*. 2020;9:100604. doi:10.1016/j.mtla.2020.100604
120. Xie H, Cao T, Gomes JV, Castro Neto AH, Rosa V. Two and three-dimensional graphene substrates to magnify osteogenic differentiation of periodontal ligament stem cells. *Carbon*. 2015;93:266–275. doi:10.1016/j.carbon.2015.05.071

International Journal of Nanomedicine

Dovepress

## Publish your work in this journal

The International Journal of Nanomedicine is an international, peer-reviewed journal focusing on the application of nanotechnology in diagnostics, therapeutics, and drug delivery systems throughout the biomedical field. This journal is indexed on PubMed Central, MedLine, CAS, SciSearch®, Current Contents®/Clinical Medicine, Journal Citation Reports/Science Edition, EMBase, Scopus and the Elsevier Bibliographic databases. The manuscript management system is completely online and includes a very quick and fair peer-review system, which is all easy to use. Visit <http://www.dovepress.com/testimonials.php> to read real quotes from published authors.

Submit your manuscript here: <https://www.dovepress.com/international-journal-of-nanomedicine-journal>